

1 Multiple negative molybdenum isotope excursions in the Doushantuo Formation
2 (South China) fingerprint complex redox-related processes in the Ediacaran
3 Nanhua Basin

4
5 Chadlin M. Ostrander^{1,*}, Swapan K. Sahoo^{2,3}, Brian Kendall⁴, Ganqing Jiang², Noah J. Planavsky⁵,
6 Timothy W. Lyons⁶, Sune G. Nielsen⁷, Jeremy D. Owens⁸, Gwyneth W. Gordon¹, Stephen J.
7 Romaniello¹, and Ariel D. Anbar^{1,9}

8
9 *1. School of Earth and Space Exploration, Arizona State University, Tempe, AZ, USA*

10 *2. Department of Geoscience, University of Nevada, Las Vegas, NV, USA*

11 *3. Equinor US, Houston, TX, USA*

12 *4. Department of Earth and Environmental Sciences, University of Waterloo, Waterloo, Ontario, Canada.*

13 *5. Department of Geology and Geophysics, Yale University, New Haven, CT, USA*

14 *6. Department of Earth Sciences, University of California, Riverside, CA, USA*

15 *7. Department of Geology and Geophysics, Woods Hole Oceanographic Institution, Woods Hole, MA, USA*

16 *8. Department of Earth, Ocean, and Atmospheric Science, National High Magnetic Field Laboratory, Florida State
17 University, Tallahassee, FL, USA*

18 *9. School of Molecular Sciences, Arizona State University, Tempe, AZ, USA*

19
20 * Correspondence to: cmostran@asu.edu

21
22 **Abstract**

23 The Ediacaran Doushantuo Formation offers one of the most complete and extensively studied
24 records of end-Neoproterozoic biotic and environmental change. Here, we report multiple coeval negative
25 molybdenum (Mo) isotope excursions (to as low as $\delta^{98}\text{Mo}_{\text{NIST}+0.25} = -2.24 \pm 0.10\%$; 2SD) in shales from
26 four separate sites in South China (Rongxi, Taoying, Wuhe, and Yuanjia) that preserve the Doushantuo
27 Formation. The negative $\delta^{98}\text{Mo}$ excursions appear coincident with previously discovered and seemingly
28 peculiar redox-sensitive element (RSE) patterns in the same sedimentary rocks. We propose that these

29 geochemical trends can be explained by some combination of (a) enhanced local marine oxygenation in
30 the sedimentary basin where the Doushantuo Formation was originally deposited (the Nanhua Basin) and
31 (b) changes in the degree of connectivity between this paleo basin and the open ocean. Enhanced local
32 marine oxygenation, by exposing more sediments in the Nanhua basin to H₂S-poor conditions, could have
33 hindered quantitative tetrathiomolybdate formation within these sediments. Local marine oxygenation
34 could have also stimulated the operation of a Mn oxide shuttle. Today, both of these processes are shown
35 to promote the retention of lighter-mass Mo isotopes in sediments and also govern RSE enrichment
36 patterns. Alternatively, or in addition, the Nanhua Basin may not have maintained an uninterrupted
37 connection with the open ocean during the Entirety of the Ediacaran Period. The negative $\delta^{98}\text{Mo}$
38 excursions occur coincident with sea level highstands that could have also exposed more sediments in the
39 basin to H₂S poor conditions and/or catalyzed the operation of a local Mn oxide shuttle. When trying to
40 infer temporal changes in ancient global ocean redox, it is important to consider the influence of sea level
41 changes and associated variations in local depositional conditions on stratigraphic trends in RSE
42 enrichments and isotope compositions.

43

44 **Main Text**

45 **1. Introduction**

46 The tempo of marine oxygenation during the Ediacaran Period (635 to 542 million years ago, or
47 Ma) is debated. It is generally accepted that the shallow ocean was oxygenated throughout the Ediacaran
48 (Lowenstein et al. 2013, and references therein). However, two predominant viewpoints exist for the O₂
49 contents of the deeper waters: (1) always anoxic (Johnston et al. 2013, Sperling et al. 2015) or (2) subject
50 to episodic ocean oxygenation events (OOEs [Fike et al. 2006, McFadden et al. 2008, Kendall et al. 2015,
51 Sahoo et al. 2012, 2016]). Resolution of this debate is important to understanding what role – if any – O₂
52 levels in Ediacaran oceans played in controlling the dynamics of early animal evolution (Knoll et al.
53 2011, Lenton et al. 2014).

54 The most commonly invoked evidence for Ediacaran OOEs comes in the form of redox-sensitive
55 element (RSE; e.g., V, Mo, Re, and U) enrichments in shales – foremost from the Doushantuo Formation
56 of South China (Sahoo et al. 2012, 2016). In the modern ocean, widespread oxygenation supports large
57 seawater reservoirs of RSE, which enables strong sedimentary RSE accumulation in the anoxic organic-
58 rich marine sediments that cover a small percentage of the ocean floor (e.g., Scott et al. 2008, Sahoo et al.
59 2012, Partin et al. 2013, Sheen et al. 2018). Intuitively, ancient black shales deposited in the primarily
60 anoxic Precambrian global ocean (Reinhard et al. 2013) and also during episodes of extensive global
61 ocean anoxia during the Cambrian (Gill et al. 2011, Owens et al. 2016) have much lower RSE abundances

62 because widespread burial in anoxic sediments depleted RSE seawater reservoirs. The transition away
63 from a predominantly anoxic Precambrian ocean and toward a well-oxygenated one more similar to
64 today's is expected to have led to first-order increases in RSE seawater reservoirs and sedimentary RSE
65 accumulation. The geochemical fingerprints of at least the initial, likely transient phases of this transition
66 seem to have been captured in black shales from the Ediacaran Doushantuo Formation (Scott et al., 2008;
67 Sahoo et al. 2012, 2016).

68 Some RSE trends in the Doushantuo Formation are peculiar, causing some researchers to
69 question their straightforward link to Ediacaran ocean oxygenation (e.g., Miller et al. 2017). For example,
70 some RSEs are enriched in Doushantuo shales to levels comparable to those found in only the most RSE-
71 enriched Phanerozoic shales (V in particular, which reaches wt. % abundances [Sahoo et al. 2016]).
72 Furthermore, during the ca. 580 Ma OOE recorded in Doushantuo shales, some RSEs are not enriched at
73 all (e.g., Mo [Sahoo et al. 2016], although pyrite from these shales is enriched in Mo [Gregory et al.
74 2017]). Lastly, the widespread ocean oxygenation implied by the episodes of RSE enrichment in the
75 Doushantuo Formation does not seem to be supported by some geochemical compilations (e.g., a recent
76 compilation of the Fe speciation record [Sperling et al. 2015]).

77 Using the Mo isotope paleoredox proxy, we provide new perspective on the sedimentary RSE
78 record from South China. The Mo isotope composition of organic-rich marine shales can be an effective
79 way to track redox changes in Earth's ancient oceans (see a recent review by Kendall et al. 2017). For
80 example, sedimentary rocks deposited under anoxic and sulfidic (hereafter referred to as euxinic)
81 conditions in restricted basins can sometimes capture the coeval seawater $\delta^{98}\text{Mo}$ (e.g., in deep portions of
82 the Black Sea [Neubert et al. 2008], Kyllaren fjord [Noordmann et al. 2015], and Lake Rogoznica [Bura-
83 Nakić et al. 2018]). Transfer of the seawater $\delta^{98}\text{Mo}$ to marine sediments is possible in these settings
84 because nearly all Mo in marine bottom waters can be transferred to underlying sediments. The Mo
85 isotope composition of seawater is a useful parameter because it is thought to be a direct consequence of
86 the relative distribution of oxic versus euxinic conditions on the seafloor (Barling et al. 2001, Arnold et al.
87 2004). For these reasons, the primary application of the Mo isotope paleoredox proxy to date has been as
88 a tool for estimating global marine redox conditions using ancient sedimentary rocks originally deposited
89 under euxinic conditions (Kendall et al. 2017).

90 In the majority of modern marine settings, however, including some that are defined as euxinic,
91 near-quantitative transfer of Mo from deep water to sediments *does not* occur and results in sedimentary
92 $\delta^{98}\text{Mo}$ that are isotopically lighter than the coeval seawater value (e.g., Arnold et al. 2004, Poulson et al.
93 2006, Poulson-Brucker et al. 2009, Nägler et al. 2011, Noordmann et al. 2015). In these settings,
94 incomplete transfer of Mo from seawater to sediments and the complexation of Mo with Fe oxide
95 minerals (Goldberg et al. 2009, 2012), Mn oxide minerals (Wasylenki et al. 2008), and organic matter

96 (King et al. 2018) – as well as the persistence of intermediate thiomolybdate species (Neubert et al. 2008)
97 – results in the preferential retention of lighter-mass Mo isotopes in these sediments. Therefore, a case can
98 be made that an important utility of the Mo isotope paleoproxy rests with tracking these processes – rather
99 than, or in addition to, its value as a proxy tracking global seawater $\delta^{98}\text{Mo}$.

100 We have measured the Mo isotope compositions of the same shale samples from the Doushantuo
101 Formation from South China that yielded the RSE evidence for OOE (i.e., those analyzed in Sahoo et al.
102 2012, 2016). Redox-sensitive elements, in addition to their sensitivity to global marine redox conditions,
103 are also sensitive to the complexation processes that affect sedimentary $\delta^{98}\text{Mo}$ (e.g., Morford et al. 1999,
104 2005, Tribovillard et al. 2006, Scholz et al. 2011, 2013, 2018). Therefore, by identifying these
105 complexation processes using Mo isotopes, we can assess their possible contribution to the RSE patterns
106 in the Doushantuo Formation.

107

108 **2. Materials and Methods**

109

110 **2.1. The Doushantuo Formation from South China**

111 We targeted shales of the Ediacaran Doushantuo Formation (~635–560 Ma [Condon et al. 2005,
112 An et al. 2015]) in multiple sections from the Yangtze platform in South China, a paleo-location referred
113 to as the Nanhua Basin (Jiang et al. 2011) (Fig. 1). In order of increasing distance from the paleo-
114 shoreline, we measured Mo isotope compositions of shales originally deposited on the continental slope
115 of the Nanhua Basin from sites at Rongxi, Taoying, and Wuhe and of shales deposited deeper within the
116 basin from the Yuanjia site. A case has been made previously that sedimentary rocks deposited in the
117 slope and basin environments of the Nanhua Basin were connected with the open ocean during deposition
118 of the Doushantuo Formation (Jiang et al. 2011, Sahoo et al. 2012).

119 We targeted shales from the entire Wuhe site (Members II through IV) and shales deposited
120 during the purported OOE from lowermost Member II (Rongxi, Taoying, and Yuanji), Member III
121 (Taoying), and Member IV (Rongxi, Taoying) of the other sections (Fig. 2). All of these sections are
122 described in detail in previous work (Jiang et al. 2011, Sahoo et al. 2012, 2016); only a very brief
123 overview is provided here.

124 Much effort has been dedicated to stratigraphically correlating the many sections from South
125 China that preserve the Doushantuo shales. For ease of correlation, the Doushantuo Formation is split into
126 four distinct members based primarily on lithology (Fig. 2). The cap carbonates overlying the glacial
127 diamictites of the Marinoan glaciation are assigned to Member I (635.2 ± 0.6 Ma [Condon et al. 2005]).
128 Cap carbonates of Member I are overlain by mixed carbonate-siliciclastics, with the onset of Member II

129 in slope sections typically signified by a transition to shale-dominated units. In the shelf and upper slope
130 sections, including the Rongxi section, Member III is dominated by carbonates, but equivalent strata in
131 the lower slope and basin sections are shale-dominated, with carbonate beds unevenly distributed in the
132 lower and upper parts. Black shales of Member IV are widespread across the entire Nanhua Basin and are
133 seen in all measured sections.

134

135 **2.2. Mo isotope methods**

136 All sample digestion, chromatography, and instrumental analysis was completed at the W. M.
137 Keck Foundation Laboratory for Environmental Biogeochemistry at Arizona State University. Whole-
138 rock powders were ashed and digested and concentrations were analyzed via quadrupole Inductively
139 Coupled Plasma Mass Spectrometry (ICPMS) using techniques outlined in previous work (Olson et al.
140 2019). Subsequently, enough sample was taken from each digested stock solution to provide 125 ng of
141 Mo, and thereafter spiked with an optimal amount of calibrated synthetic Mo isotope double spike (^{97}Mo
142 and ^{100}Mo) to correct for isotopic fractionation during chromatography and for instrumental mass bias
143 (Siebert et al. 2001). Molybdenum purification involved the typical two-step anion and cation column
144 procedure (e.g., Duan et al. 2010).

145 Isotope ratio measurements were performed on a Thermo Neptune multi-collector ICPMS (MC-
146 ICPMS) in low-resolution mode with an Elemental Scientific Inc. Apex inlet system and using sample-
147 standard bracketing. All measurements were made using the Johnson Matthey Specpure Mo plasma
148 standard (Lot #802309E; RochMo2) as the bracketing standard and then re-calculated relative to the new
149 international NIST SRM 3134 standard = + 0.25‰ (Nägler et al. 2014). In brief, the measured value for
150 NIST SRM 3134 was $0.33 \pm 0.04\%$; 2SD relative to RochMo2 during our analytical sessions (Table 1).
151 Accordingly, 0.08‰ was subtracted from each sample Mo isotope composition measured relative to
152 RochMo2. Samples and standards were analyzed at a concentration of 25 ng/g Mo, which yielded about
153 three volts of signal on mass 98. Samples were analyzed in duplicate (at least), with the average 2SD
154 sample reproducibility being 0.05‰ and the maximum being 0.22‰. Over the period of Mo isotope
155 analysis for this study, USGS rock reference material SDO-1 (Devonian Ohio Shale) was simultaneously
156 processed with each batch of samples to monitor accuracy and showed good reproducibility ($\delta^{98}\text{Mo} =$
157 $1.07 \pm 0.05\%$; 2SD; compared to $1.05 \pm 0.14\%$; 2SD; in previous work [Goldberg et al. 2013]) as did
158 multiple secondary standard solutions (Table 1). Lastly, for each analytical run, a series of standards with
159 varying spike-sample ratios was measured. All samples were within the validated spike-sample range for
160 accurate and precise $\delta^{98}\text{Mo}$ values.

Table 1. Mo isotope data from standard reference material solutions

Standard	$\delta^{98}\text{Mo}$ (2SD) ^a	N	Normalized to NIST + 0.25‰	Goldberg et al. (2013)
ICL-Mo	0.18 (0.04)	21	0.10 (0.04)	0.09 (0.05)
Kyoto-Mo	-0.03 (0.06)	5	-0.11 (0.06)	-0.12 (0.06)
NIST SRM 3134	0.33 (0.04)	42	0.25	0.25
SDO-1	1.14 (0.05)	35	1.06 (0.05)	1.05 (0.14)

a. measured relative to Roch-Mo2

*all reported errors are 2SD of the standard reproducibility

162

163

164 3. Results

165 Molybdenum isotope compositions in shales of the Doushantuo Formation from all slope and
 166 basin sections across the purported OOE (i.e., in Doushantuo Members II, III, and IV) are predominantly
 167 negative (as low as $-2.24 \pm 0.10\text{‰}$; 2SD; in Member II of the Taoying section) (Fig. 3 and 4). The
 168 heaviest measured shale $\delta^{98}\text{Mo}$ during the OOE is $1.32 \pm 0.15\text{‰}$ (2SD) and comes from Member IV of
 169 the Rongxi section. Maximum $\delta^{98}\text{Mo}$ in shales deposited during the older OOE are isotopically lighter:
 170 $0.76 \pm 0.10\text{‰}$ during the OOE in lower Member II (again from the Rongxi section) and $0.78 \pm 0.10\text{‰}$
 171 during the OOE in lower Member III (from the Taoying section).

172 In contrast, $\delta^{98}\text{Mo}$ in shales from the Wuhe section between the OOE are always positive (Fig.
 173 3). One sample from uppermost Member III from this section (110.7 m) is especially heavy ($2.24 \pm$
 174 0.10‰ ; 2SD). Other than this one sample, $\delta^{98}\text{Mo}$ values are much lighter, exceeding 1.0‰ only one other
 175 time ($1.47 \pm 0.10\text{‰}$; 2SD; in lowermost Member II immediately above the oldest OOE) and remain fairly
 176 invariant otherwise ($\delta^{98}\text{Mo} = 0.57 \pm 0.21\text{‰}$; 2SD).

177

178 4. Discussion

179 In the following section, we begin by first discussing local processes in the Ediacaran Nanhua
 180 Basin that most likely played a role in driving the observed negative Mo isotope compositions in the
 181 Doushantuo Formation (**Section 4.1**). We then discuss how these local processes likely also played some
 182 role in governing the RSE patterns found in shales of the Doushantuo Formation (**Section 4.2**). Lastly, we
 183 finish this section by discussing a combination of plausible scenarios that may account for the transient
 184 nature of the geochemical excursions found in the Doushantuo Formation (**Sections 4.3 and 4.4**).

185

186 4.1. Negative $\delta^{98}\text{Mo}$ in Doushantuo shales

187 Negative $\delta^{98}\text{Mo}$ that are well below crustal estimates cannot represent Ediacaran global open-
188 ocean seawater. The estimated average $\delta^{98}\text{Mo}$ of upper crustal rocks covers a restricted range between
189 about 0.35‰ and 0.60‰ (Willbold and Elliot 2017). Because the vast majority of Mo delivered to the
190 ocean is sourced from crustal rocks (Miller et al. 2011, Greaney et al. 2018) and because all processes that
191 operate during Mo delivery to and removal from the ocean preferentially retain lighter-mass Mo isotopes,
192 the seawater $\delta^{98}\text{Mo}$ at any time in Earth's history was probably never lighter than this crustal composition
193 (reviewed in Kendall et al. 2017).

194 Only two processes in modern marine settings are capable of driving the large negative Mo
195 isotope fractionation effects observed in the Doushantuo Formation: delivery of lighter-mass Mo isotopes
196 to sediments by (1) Mn oxide minerals (i.e., a Mo shuttle [Scholz et al. 2013, 2018]) and (2)
197 thiomolybdates (Tossel 2005, Neubert et al. 2008). The operation of one or both of these processes in the
198 Ediacaran Nanhua Basin must have led to the preservation of a sedimentary $\delta^{98}\text{Mo}$ much lighter than the
199 ancient seawater composition.

200

201 **4.1.1. “Shuttling” by Mn oxide minerals**

202 The transient development of a Mn oxide “shuttle” in the Ediacaran Nanhua Basin could help
203 explain the negative $\delta^{98}\text{Mo}$ excursions in shales from the Doushantuo Formation. Today, the most well-
204 studied marine basin hosting a Mn oxide shuttle is the Baltic Sea (e.g., Scholz et al. 2013, 2018, Hardisty
205 et al. 2016). In the Baltic Sea, during transient introduction of well-oxygenated waters into the semi-
206 restricted basin, insoluble Mn oxides form high in the water column and sink to the seafloor (Huckriede
207 and Meischner 1996). Upon being introduced to the anoxic and euxinic conditions deeper in the water
208 column or underlying sulfidic sediments, these same Mn oxides are solubilized during reductive
209 dissolution, typically evading burial in marine sediments if O_2 is not present in bottom waters (Calvert
210 and Pedersen 1996, Häusler et al. 2018). Some RSEs bound to Mn oxides are retained in sediments after
211 reductive dissolution, however, because they are less soluble under the reducing conditions present in
212 bottom waters and sediments (e.g., Mo and V [Morford et al. 2005, Scholz et al. 2011, 2013]). In the case
213 of Mo, the presence of appreciable hydrogen sulfide is required to promote sedimentary retention
214 (Crusius et al. 1996, Morford et al. 2005). When Mo is shuttled by Mn oxides from oxic surface waters of
215 the Baltic Sea to underlying sulfidic sediments, these sediments have $\delta^{98}\text{Mo}$ nearly 3.0‰ lighter than the
216 overlying seawater value (Scholz et al. 2013, 2018), similar to the equilibrium isotope effect imparted
217 during Mo sorption to Mn oxides ($\Delta^{98}\text{Mo} = 2.7 \pm 0.1\%$ [Wasylenki et al. 2008]).

218 In comparison, sediments that receive lighter-mass Mo isotopes via an Fe oxide shuttle have an
219 authigenic $\delta^{98}\text{Mo}$ only ~1.0‰ lighter than the overlying seawater value (e.g., those from the geologically
220 recent Peruvian continental margin [Scholz et al. 2017]). This smaller isotopic offset is similar to that

221 imparted during Mo sorption to ferrihydrite and goethite ($\Delta^{98}\text{Mo} = 1.11 \pm 0.15\text{‰}$ and $\Delta^{98}\text{Mo} = 1.40 \pm$
222 0.48‰ , respectively [Goldberg et al. 2009]), Fe oxide minerals shown to be abundant in particulate matter
223 of the modern Peruvian margin oxygen minimum zone (Scholz et al. 2017). Given the magnitude of the
224 $\delta^{98}\text{Mo}$ excursions found here in shales of the Doushantuo Formation (to as low as $\delta^{98}\text{Mo}_{\text{NIST}+0.25} = -2.24 \pm$
225 0.10‰ ; 2SD), it is unlikely that the sediments were strongly affected by an Fe oxide shuttle. More likely,
226 the extremely light $\delta^{98}\text{Mo}$ require the larger Mo isotope fractionation effects associated with adsorption to
227 Mn oxides ($\Delta^{98}\text{Mo} = 2.7 \pm 0.1\text{‰}$ [Wasylenki et al. 2008]).

228 Large V enrichments in shales from the Doushantuo Formation support the operation of an oxide
229 shuttle in the Nanhua Basin. These shales are dramatically enriched in V (up to ~ 3 wt% [Sahoo et al.
230 2016]), more so than any modern marine sediments (all < 0.05 wt% [Nameroff et al. 2002, Scholz et al.
231 2011]). In fact, the exceptional enrichments have been cited as challenging the original interpretation
232 linking RSE enrichments to OOEes (Miller et al. 2017) and attributed instead to poorly understood
233 secondary enrichment processes. Notably, V possesses a particularly strong affinity for oxide minerals
234 and is consequently highly enriched in ferromanganese crusts (up to 0.08 wt% [Hein and Koschinsky
235 2014]) relative to its abundance in seawater (35 nmol/L [Collier 1984]), much more so than most other
236 RSEs (Fig. 5). Modern anoxic marine sediments that receive RSE-laden oxides from overlying oxic
237 waters, or those that form oxides in-situ during seasonal inflow of oxygenated waters, also become
238 enriched in V (up to 0.04 wt% [e.g., Morford et al. 2005, Scholz et al. 2011]). A general negative
239 correlation between V_{EF} and $\delta^{98}\text{Mo}$ ($R^2 = 0.59$; Fig. 6) is consistent with co-delivery of V and lighter-
240 mass Mo isotopes via a Mn-oxide shuttle. This relationship is not as apparent between $\delta^{98}\text{Mo}$ and EFs for
241 RSEs with a relatively lower affinity for oxide minerals (Mo_{EF} [$R^2 = 0.12$] and U_{EF} [$R^2 = 0.19$]; Fig. 6).

242 An alternate means of promoting V hyper-enrichment, recently proposed by Scott et al. (2017), is
243 unlikely to have driven the strong V enrichments in the Doushantuo Formation. Scott et al. (2017)
244 attribute strong V enrichments (up to 0.25 wt%) in organic-rich shales from the Late Devonian-Early
245 Mississippian Bakken Formation to extremely high levels of H_2S (to >10 mM) in the original bottom
246 waters or sediments. This hypothesis is supported by strong enrichment of Mo in the same shale samples
247 (up to 0.18 wt%) because sedimentary Mo accumulation today is enhanced in H_2S -rich settings (Crusius
248 et al. 1996, Morford et al. 2005). In the Doushantuo Formation, however, the most V-enriched shales (up
249 to single wt% during OOE “B” in the Wuhe section; see Fig. 3) have very low Mo abundances (reaching
250 only 15 $\mu\text{g/g}$). Furthermore, Fe speciation ratios in these shales, as well as those deposited during OOE
251 “A” where V abundances are also very high (up to 0.4 - 0.6 wt% at the Taoying, Wuhe, and Yuanji sites),
252 often dip below the thresholds for euxinic deposition (see Figs. 3 and 4). These geochemical fingerprints
253 are inconsistent with the H_2S -replete conditions required by the Scott et al. (2017) hypothesis. Therefore,

254 although this mechanism of V hyper-enrichments may explain the Bakken Formation data, it is not
255 supported by the geochemical trends in the Doushantuo Formation.

256 Operation of an oxide shuttle during the OOE is also suggested when viewed using a more
257 classical method of identification – that is, preferential sedimentary accumulation of Mo over U under
258 sulfidic conditions (Algeo and Tribouillard 2009). During the operation of a local oxide shuttle, Mo can
259 accumulate in sulfidic marine sediments much more efficiently than U because scavenging of Mo by
260 oxide minerals is stronger than scavenging of U by oxide minerals (apparent in Fig. 5). Consistent with
261 this model, Mo enrichments in Doushantuo shales during the OOE are sometimes much greater than U
262 when $\delta^{98}\text{Mo}$ are very negative (Fig. 7). Some shale samples with very negative $\delta^{98}\text{Mo}$ do not exhibit this
263 Mo-U enrichment pattern, however, requiring an alternative explanation (see section 4.1.2).

264 Importantly, muted Mn contents in bulk shale samples throughout the Doushantuo Formation
265 from all sections studied here do not preclude the shuttle hypothesis (never above 0.24 wt% Mn relative
266 to the average upper continental crust value of 0.08 wt% [Rudnick and Gao 2003]; see Supplementary
267 Data Table). Although sedimentary RSE enrichments are an expected consequence of an oxide shuttle,
268 sedimentary Mn accumulation is not. Manganese is highly soluble after reductive dissolution under
269 anoxic or euxinic conditions (as Mn^{2+}) and does not readily form sulfide minerals (Burdige 1993). A
270 persistent presence of free O_2 in marine bottom waters is required to promote appreciable Mn
271 accumulation in marine sediments (Calvert and Pedersen 1996, Häusler et al. 2018). Previous attempts to
272 constrain local marine redox conditions on the slope of and within the deeper portions of the Nanhua
273 Basin found evidence for either euxinic, anoxic, or suboxic conditions (e.g., Wang et al. 2012, Sahoo et
274 al. 2012, 2016, Jin et al. 2018), all of which do not favor Mn accumulation. Even under the most
275 oxidizing of these conditions (i.e., suboxic), O_2 may not sufficiently penetrate marine sediments to
276 support Mn retention (Morford et al. 2005). Thus, there is no reason to expect Mn enrichments in shales
277 of the Doushantuo Formation despite the likely delivery of Mo via Mn oxides. Notably, individual pyrite
278 grains from shales of the Doushantuo Formation deposited during OOE are slightly enriched in Mn (but
279 <1.0 wt% [Gregory et al. 2017]). These slightly elevated abundances might fingerprint the intense
280 (re)cycling of Mn that took place in the original bottom waters or sediments, especially given the low
281 affinity of Mn for sulfide (Burdige 1993).

282

283 **4.1.2. Incomplete tetrathiomolybdate formation**

284 When transfer of Mo from seawater into sediments is non-quantitative, a large isotopic offset can
285 result from the formation of thiomolybdate ions (i.e., $\text{MoO}_x\text{S}_{4-x}^{2-}$), an offset that can leave sediments
286 dramatically enriched in lighter-mass Mo isotopes (Tossell 2005, Neubert et al. 2008, Nägler et al. 2011).
287 Thiomolybdate ions form in the presence of hydrogen sulfide. In marine settings where hydrogen sulfide

288 is abundant in marine bottom waters and sediments ($>11 \text{ uM H}_2\text{S}_{(aq)}$), the predominant thiomolybdate
289 formed is tetrathiomolybdate (MoS_4^{2-} [Erickson and Helz 2000]). In marine settings where sulfide
290 availability is low and/or unstable (i.e., where local marine bottom waters are only weakly or transiently
291 euxinic, anoxic and non-sulfidic, or weakly oxygenated), however, conversion of molybdate to
292 tetrathiomolybdate is incomplete and leads to the formation of thiomolybdate intermediates with very
293 different Mo isotope compositions (mono- ($\text{MoO}_3\text{S}_1^{2-}$), di- ($\text{MoO}_2\text{S}_2^{2-}$), and tri- ($\text{MoO}_1\text{S}_3^{2-}$)
294 thiomolybdates [Tossell 2005]). In the most extreme case found to date, sedimentary $\delta^{98}\text{Mo}$ thought to be
295 a product of incomplete tetrathiomolybdate formation are up to $\sim 3\%$ lighter than the seawater
296 composition (immediately below the chemocline of the Black Sea [Neubert et al. 2008, Nägler et al.
297 2011]).

298 Similar to the identification of an oxide shuttle, variations in sedimentary Mo-U patterns may also
299 be used to identify conditions unfavorable for quantitative tetrathiomolybdate transformation (e.g.,
300 Azrieli-Tal et al. 2014). Fluctuations in ancient localized hydrogen sulfide contents are thought to be
301 fingerprinted in shales by progressive increases (more sulfidic) and decreases (less sulfidic) in the
302 enrichments of both Mo and U (Algeo and Tribovillard 2009). This pattern results from the shared
303 affinity of both RSEs for reducing conditions, affinities that strengthen steadily as conditions become
304 more reducing in marine bottom waters and sediments. Indeed, many of the Doushantuo shales with very
305 negative $\delta^{98}\text{Mo}$ plot along a line of increasing Mo and U (Fig. 7). This relationship is an expected
306 consequence of an ancient, relatively open-marine environment where redox conditions fluctuated
307 between suboxic, anoxic, and euxinic deposition. Iron speciation ratios reported in previous work
308 corroborate this suggestion (Sahoo et al. 2012, 2016). At times during the purported OOE, $\text{Fe}_{\text{HR}}/\text{Fe}_{\text{T}}$ and
309 $\text{Fe}_{\text{PY}}/\text{Fe}_{\text{HR}}$ ratios in all sections show variations consistent with deposition from oxic, anoxic, and euxinic
310 bottom waters (Figs. 3 and 4). These variations in local redox conditions, particularly away from euxinia,
311 would have promoted incomplete tetrathiomolybdate formation in the original sediments, resulting in the
312 preferential retention of lighter-mass Mo isotopes.

313 Notably, some Doushantuo shale samples still plot outside of the suboxic-anoxic-euxinic and
314 oxide shuttle fields in Fig. 7. Shales that plot between these two fields may be explained by some
315 combination of fluctuations in local redox conditions (i.e., between suboxic, anoxic, and euxinic) and the
316 operation of an oxide shuttle. The four shale samples from the Taoying site that plot to the right of the
317 suboxic-anoxic-euxinic field (i.e., those with much higher U_{EF} relative to Mo_{EF} ; Fig. 7), however, may
318 still require an alternative explanation. Nonetheless, with the exception of these four samples, all other
319 Doushantuo shales plot within or between the suboxic-anoxic-euxinic and oxide shuttle fields. Therefore,
320 the local processes these $\text{Mo}_{\text{EF}}\text{-U}_{\text{EF}}$ patterns signify likely played the most significant role in driving the
321 geochemical trends found in Doushantuo shales deposited during the purported OOE.

322

323 **4.2. A reappraisal of RSE trends in the Doushantuo Formation during OOE**

324 The processes outlined in the preceding section, in addition to driving light sedimentary $\delta^{98}\text{Mo}$,
325 are known to have a profound effect on sedimentary RSE abundances. In this light, the RSE patterns in
326 the Doushantuo Formation during the purported OOE need to be re-assessed.

327

328 **4.2.1. Links to other local processes in the Nanhua Basin**

329 Sedimentary RSE enrichments today, in addition to being affected by oxide shuttling, are heavily
330 dependent on local redox conditions. This dependency must have also been present in ancient marine
331 sedimentary environments (summarized in Tribovillard et al. 2006). Of the RSEs highlighted here, V, Re,
332 and U are all preferentially retained in sediments under anoxic conditions. Molybdenum, however, is not
333 retained in sediments unless dissolved sulfide contents in marine bottom waters or sediment pore waters
334 are comparatively high (Crusius et al. 1996, Morford et al. 2005). This well-documented link between Mo
335 and sulfide is supported by the RSE data from the Doushantuo Formation during the OOE. Specifically,
336 Doushantuo shale samples with $\text{Fe}_{\text{HR}}/\text{Fe}_{\text{T}}$ and $\text{Fe}_{\text{Py}}/\text{Fe}_{\text{HR}}$ ratios indicative of euxinic deposition (i.e.,
337 $\text{Fe}_{\text{HR}}/\text{Fe}_{\text{T}} > 0.22$ and $\text{Fe}_{\text{Py}}/\text{Fe}_{\text{HR}} > 0.80$ [Raiswell et al. 2018]) have more pronounced Mo enrichments (in
338 particular, shales from OOE A and C; Fig. 8). These differences in the abundance of Mo between shales
339 deposited under euxinic versus non-euxinic conditions (p -value = 0.000004 for a two-tailed and unpaired
340 t -test) are greater than those observed for the other RSEs (p -value = 0.04 for U, 0.08 for V, and 0.12 for
341 Re using the same test). Furthermore, Mo abundances are elevated in spheroidal pyrite grains throughout
342 the Wuhe section, particularly during OOE (Gregory et al. 2017). Together, these relationships support
343 the idea that sedimentary Mo retention in the Doushantuo Formation was coupled to sulfide in the water
344 column and sediments.

345 While, in general, shale Mo abundances during OOE are greater when Fe speciation indicates
346 deposition occurred under at least locally euxinic conditions, there are still clear exceptions to this rule.
347 For example, a few shale samples deposited under euxinic conditions according to the Fe data possess
348 very low Mo abundances (e.g., as low as 2 $\mu\text{g/g}$ in the Wuhe section during OOE “B”), while some
349 deposited under predominantly non-euxinic conditions based on the Fe data possess much higher Mo
350 abundances (e.g., as high as 81 $\mu\text{g/g}$ in the Rongxi section during OOE “C”). There are multiple possible
351 explanations for these outliers. For example, local depositional controls in the paleo-basin, such as the
352 availability and type of organic matter (Algeo and Lyons 2006), sedimentary carbonate content, and
353 sedimentation rates (Hardisty et al. 2018), would have influenced the sedimentary Mo abundances (as
354 well as the other RSE abundances). Furthermore, each OOE represents roughly a duration of 5 to 10

355 million years (Sahoo et al. 2016). As such, fluctuations in global marine redox conditions within and
356 especially between these events are possible, indeed likely, and could have played an important role in
357 regulating sedimentary Mo abundances. Changes in the degree of connection between the Nanhua Basin
358 and the open ocean, if this occurred over million-year timescales, would have also played a strong role in
359 regulating the abundance of Mo in seawater and sediments of the basin (Algeo and Lyons 2006).

360

361 4.2.2. Links to global ocean oxygenation

362 In modern marine sediments, Re and U, unlike Mo and V, are largely unaffected by oxide
363 shuttling (Morford et al. 2005, Algeo and Tribovillard 2009), and therefore their high abundances in black
364 shales from the Doushantuo Formation are probably linked to extensive global ocean oxygenation. The
365 only known way to enhance sedimentary Re and U abundances to Phanerozoic levels, such as is found
366 during Ediacaran OOE in the Doushantuo Formation, is by increasing ocean oxygenation and in turn
367 expanding the size of their global seawater reservoirs (Partin et al. 2013, Sheen et al. 2018). This general
368 relationship is evident in the ancient shale record, where both Re and U abundances are predominantly
369 low in shales from the Precambrian but show a first-order increase across the Ediacaran-Cambrian
370 boundary in response to an overall trend towards higher ocean O₂ levels in the Phanerozoic Eon (Partin et
371 al. 2013, Sheen et al. 2018).

372 The combined effects of a local Mn oxide shuttle and global-scale OOE may explain why
373 sedimentary RSE enrichments in the Doushantuo Formation are so high, sometimes exceeding those
374 found in modern marine sediments. Large-scale OOE during the Ediacaran Period would have increased
375 RSE reservoirs, while at the same time also stimulating RSE delivery to sedimentary environments
376 hosting an oxide shuttle. These combined effects are apparent when shale V and Re abundances from the
377 Doushantuo Formation during OOE are plotted against one another and reveal a general correlation (R^2
378 = 0.38; Fig. 9). High sedimentary Re abundances in the Doushantuo Formation require global ocean
379 oxygenation (Sheen et al. 2018), while high sedimentary V abundances may be best explained by
380 supplementation via a local oxide shuttle (see **Section 4.1.1**). Therefore, the correlation between these two
381 elements is an indication that both processes may have been operating in unison.

382 Molybdenum isotope compositions reported in this study for the Doushantuo Formation during
383 the purported OOE, despite the described complications and the exceptionally light values, could still be
384 evidence for a better-oxygenated Neoproterozoic ocean. At multiple times during the Phanerozoic Eon,
385 such as during some Mesozoic Oceanic Anoxic Events (OAEs), the seawater $\delta^{98}\text{Mo}$ is estimated to have
386 been much lower than that of the modern ocean ($\delta^{98}\text{Mo}_{\text{SW}} = \sim 1.45\%$ during both the Toarcian OAE and

387 Cenomanian-Turonian OAE-2 [summarized in Dickson 2017]). Paleoproxy evidence suggests that
388 Earth's deep open ocean remained mostly oxygenated during these OAEs, with deoxygenation taking
389 place primarily in shallow shelf and margin environments (< 10% of the global seafloor [Owens et al.
390 2013, Dickson et al. 2016, Clarkson et al. 2018]). Large RSE enrichments are preserved in sedimentary
391 rocks deposited during these events despite the large scale of marine deoxygenation and accompanying
392 decline in seawater $\delta^{98}\text{Mo}$ (e.g., Mo concentrations in the hundreds of $\mu\text{g/g}$ and V in the thousands
393 [Hetzl et al. 2009, Owens et al. 2012, Owens et al. 2016]). In short, a seawater $\delta^{98}\text{Mo}$ during Ediacaran
394 OOE lower than that of the modern ocean is not inconsistent with the OOE hypothesis. Ocean
395 oxygenation during the Ediacaran OOE could have been greater than those present during most of the
396 Proterozoic Eon – and perhaps comparable to ocean oxygenation levels during Mesozoic OAEs.

397 General agreement between the levels of predicted ocean oxygenation during Ediacaran OOE
398 and the Mesozoic OAEs could even be supported by the worldwide Neoproterozoic Fe speciation record
399 (Sperling et al. 2015). When originally presented, these Fe data were interpreted in the opposite way – as
400 being contradictory to the OOE hypothesis. Sperling et al. (2015) argued for predominantly anoxic global
401 marine margins throughout the Neoproterozoic. These authors were limited to predictions for marine
402 margin settings because Neoproterozoic shales on or near Earth's surface today were deposited
403 predominantly in these proximal and relatively shallow settings (that is, a preservational bias leads to a
404 sampling bias). During Mesozoic OAEs, pronounced ocean deoxygenation was most prevalent in
405 marginal environments because of the higher biological production in these regions (Dickson et al. 2016,
406 Owens et al. 2013, Owens et al. 2018). Therefore, in an ocean with redox conditions similar to those
407 Mesozoic OAEs, margin settings may very well have been predominantly anoxic, despite increasing
408 oxygenation away from those margins. If correct, this model would allow for the persistence of anoxia
409 suggested in the Sperling et al. (2015) data along the margins, while still allowing for a well-oxygenated
410 deep open ocean.

411

412 **4.3. Transiency of negative $\delta^{98}\text{Mo}$ and strong RSE enrichments**

413 Equally impressive as the magnitude of negative $\delta^{98}\text{Mo}$ and RSE enrichments in shales of the
414 Doushantuo Formation is their transient and seemingly episodic appearance. The short-lived nature of
415 these excursions (<5-10 million years [Sahoo et al. 2016]) may fingerprint major changes that occurred to
416 the Nanhua Basin if not the global ocean during the Ediacaran.

417 We present two hypotheses: the transient nature of the geochemical trends found in the
418 Doushantuo Formation may have been a result of some combination of (1) changes in the position of the

419 local chemocline and/or (2) dramatic changes in global sea level. Critically, neither of these hypotheses
420 can at present be ruled out as a contributing factor to the episodic geochemical trends. Furthermore, these
421 hypotheses are not mutually exclusive; changes in the position of the local chemocline can be modulated
422 by global sea level changes. For these reasons, we highlight here the evidence in support of each
423 hypothesis and discuss some of the associated implications.

424

425 **4.3.1. Links to chemocline fluctuations**

426 A deepening of the chemocline in the Nanhua Basin during OOE's could help explain the
427 geochemical trends found in the Doushantuo Formation. Deepening of the chemocline would have
428 exposed more sediments on at least the slope of the Nanhua Basin, and potentially sediments deposited
429 deeper within the basin (i.e., at the Yuanjia site), to oxic or suboxic bottom waters (e.g., Han and Fan
430 2015). Manganese oxide minerals formed in these bottom waters, as well as higher in the water column,
431 could then have shuttled RSEs to the marine sediments. Again, because Mn contents are muted in all
432 shale samples analyzed here, O₂ in marine bottom waters at the studied localities probably did not
433 penetrate deep enough into underlying sediments to promote Mn retention in these settings (i.e.,
434 conditions in sedimentary pore waters probably only reached suboxic; see **Section 4.1.1.**). An additional
435 consequence of more oxidizing marine bottom waters above the original Nanhua Basin sediments would
436 be a decrease in the availability of labile organic matter, which would have suppressed accumulation of
437 sulfide in pore waters. By association, incomplete sedimentary tetrathiomolybdate formation could also
438 have been promoted by deepening of the chemocline. The coupled effects from a local Mn oxide shuttle
439 and incomplete tetrathiomolybdate formation, as a result of a deepening chemocline in the Nanhua Basin,
440 could have promoted retention of lighter-mass Mo isotopes in the original sediments.

441 Deepening of the chemocline during OOE's need not have been restricted to the Nanhua Basin,
442 and instead this phenomenon may have occurred over large areas of Ediacaran global oceans. In fact, the
443 original OOE hypothesis predicts this based on the requirement of enhanced global ocean oxygenation to
444 drive the dramatic increase in each seawater RSE reservoir (Sahoo et al. 2012, 2016). Proterozoic oceans
445 are thought to have been predominantly anoxic, with oxic conditions restricted primarily to shallow
446 settings (e.g., Reinhard et al. 2013, 2016). In comparison, Ediacaran oceans during OOE's are thought to
447 have been better oxygenated, with oxic conditions being commonly present also in much deeper settings.

448 If the local chemocline did deepen in the Ediacaran Nanhua Basin during the purported OOE's,
449 then this phenomenon may have been linked to localized physical processes. For example, strengthened
450 wind speeds can drive deeper local pycnoclines, and by extension also deeper chemoclines. Likewise, the
451 formation of local bottom waters could have driven the same effect because, since these waters would

452 have been very dense and O₂-rich, they would have introduced O₂ to greater depths in the water column
453 (as has happened multiple times over the past few decades in areas of the Mediterranean Sea [Schneider
454 et al. 2014]). The transient development of one or both of these localized physical processes in the
455 Ediacaran Nanhua Basin may therefore have been a major factor in driving the negative δ⁹⁸Mo excursions
456 and coeval RSE patterns found in the Doushantuo Formation.

457

458 **4.3.2. Links to changes in global sea level**

459 The episodic geochemical trends found in the Doushantuo Formation could also have been
460 stimulated by global sea level change during the Ediacaran. Marine regressions and transgressions show a
461 strong link to the geochemical trends in the Doushantuo Formation (apparent in Fig. 3), and these
462 dramatic changes in sea level have been invoked in previous work to explain other geochemical patterns
463 in the Doushantuo Formation (Och et al. 2016).

464 Some of the geochemical trends found between the purported OOE in Doushantuo shales from
465 the Wuhe section, although not originally interpreted in this manner (Sahoo et al. 2016), could be linked
466 to a loss in connection between the Nanhua Basin and the open ocean. A prevalence of the clay mineral
467 saponite in sedimentary rocks from the Jiulongwan section from South China was interpreted as evidence
468 for a shelf lagoon in the Nanhua Basin (see Fig. 1) that was strongly restricted during deposition of
469 Members I and II of the Doushantuo Formation (Bristow et al. 2009; but also see Huang et al. 2013 for an
470 alternative explanation of this data). Anomalously low RSE concentrations in sedimentary rocks of the
471 Jiulongwan section (Mo and U abundances of ~ 2 μg/g) were interpreted as corroborative evidence for a
472 restricted setting with limited RSE input from open ocean seawater (Bristow et al. 2009). Similar to the
473 findings of Bristow et al. (2009), RSE abundances in the Wuhe section outside of the purported OOE are
474 also extremely low (Mo and U, for example, are often < 2 μg/g [Sahoo et al. 2016]) and may thus be
475 interpreted in the same way. Importantly, the degree of restriction on the slope and in the deeper basin
476 need not have been as severe as that experienced by the shelf lagoon. Isolation of the shelf lagoon during
477 deposition of Members I and II of the Doushantuo Formation is postulated to have been sufficiently
478 strong to promote a lacustrine environment (Bristow et al. 2009; but also see Huang et al. 2013), but
479 coeval sections at this time deposited in the basin probably maintained some connection to the open ocean
480 (Bristow et al. 2009).

481 Evidence for a semi-restricted Nanhua Basin between the purported OOE is not limited to low
482 RSE abundances. For instance, local reservoir effects in highly restricted euxinic environments today with
483 very low seawater sulfate concentrations prevent transfer of the large negative S isotope fractionation
484 effects induced during microbial sulfate reduction to sediments of those basins (Gomez and Hurtgen

485 2015). Positive pyrite S isotope compositions between OOE's in the Wuhe section (Sahoo et al. 2016)
486 could therefore also be explained by the development of basinal restriction. Basinal restriction may also
487 help explain why sediments from the Wuhe site were deposited under a persistently euxinic water column
488 between the OOE's (according to Fe speciation data; Fig. 3). Modern restricted basins where inflow of
489 nutrient- and O₂-rich marine bottom waters is limited are also often euxinic (Meyer and Kump 2008). It is
490 worth noting, however, that modern restricted basins are probably more susceptible to the development of
491 euxinic conditions than were restricted basins during the Ediacaran because of the higher abundance of
492 sulfate in modern seawater. Furthermore, a strong surface-to-deep carbon (C) isotope gradient in the
493 Ediacaran Nanhua Basin between the OOE's has been inferred from systematic differences in the
494 carbonate and organic C isotope profiles from various sections in South China (e.g., Jiang et al. 2007,
495 Wang et al. 2016). Strong surface-to-deep C isotope gradients are found today in restricted redox-
496 stratified basins (e.g., the Black Sea and Framvaren Fjord [Volkov 2000]). Finally, independent evidence
497 for regression and development of sea-level lowstands (e.g., the appearance of cross-laminations in
498 carbonates from South China [McFadden et al. 2008]) coincides with the periods between OOE's
499 (apparent in Fig 3) and may have favored basin restriction. Many basins are likely to lose at least some
500 connectivity with the open ocean during sea level lowstands.

501 Like the correlation between marine regressions and the intervals between the OOE's, the
502 correlation between marine transgressions and the OOE's themselves may also not be coincidental. In fact,
503 marine transgression, by improving connection between the Ediacaran Nanhua Basin and the open ocean,
504 provides a means of catalyzing a vigorous Mn oxide shuttle and bringing metals into the basin. In the
505 modern Baltic Sea, the operation of a Mn oxide shuttle is catalyzed in a similar manner – that is, by the
506 transient introduction of well-oxygenated waters into the semi-restricted basin (Huckriede and Meischner
507 1996). We propose that times of transient inflow of well-oxygenated Ediacaran ocean surface waters to a
508 Nanhua Basin that was better connected to the open ocean stimulated a Mn oxide shuttle similar to that
509 observed in the modern Baltic Sea. During these inflow events, rapid accumulation of isotopically light
510 Mo, as well as many other RSEs, would have occurred in euxinic sediments of the basin.

511 Some key differences do exist between the geochemistry of sediments from the recent Baltic Sea
512 and that preserved in the Doushantuo Formation. For example, Mn contents reach much higher values in
513 geologically recent Baltic Sea sediments compared to those of the Doushantuo Formation (~15 wt%
514 [Hardisty et al. 2016] versus <1.0 wt% [Sahoo et al. 2016], respectively). We could explain this disparity
515 by inflow events into the Ediacaran Nanhua Basin that were sporadic or of weaker intensity relative to
516 those occurring recently in the Baltic Sea. The presence of O₂ in marine bottom waters and its ability to
517 catalyze Mn oxide formation in underlying sediments is likely a prerequisite for sedimentary Mn

518 accumulation (Calvert and Pedersen 1996). In support of this assumption, sedimentary Mn accumulation
519 in the Baltic Sea is limited during inflow events that occur sporadically over extremely short timescales
520 (e.g., a single year) because penetration of O₂ into marine bottom waters occurs over correspondingly
521 short timescales and leads to only limited Mn oxide formation (Heiser et al. 2001, Lenz et al. 2015). By
522 analogy, Ediacaran sediments are not expected to have accumulated Mn if O₂ penetration into deep
523 marine waters of the local sedimentary basin was sporadic or if O₂ failed to penetrate into the deep waters
524 of the basin.

525

526 **4.4. Implications of basinal restriction between the OOE's**

527 A weakened connection between the Nanhua Basin and the open ocean during the intervals
528 between the purported OOE's would have had profound consequences on the geochemistry of the basin.
529 Today, a poor connection between the Black Sea and the open ocean inhibits delivery of Mo to this basin
530 (Eckert et al. 2013). Consequently, the availability of Mo in bottom waters and also its burial flux in
531 organic-rich sediments of the modern Black Sea are not as pronounced as those observed in anoxic basins
532 better connected to the open ocean (e.g., the Cariaco Basin [Algeo and Lyons 2006]). Knowing this, it
533 becomes apparent that shale Mo abundances between the purported OOE's may undersell the true size of
534 the coeval global seawater Mo inventory if the basin was poorly connected to the open ocean at these
535 times. Additionally, it has been shown that organic-rich marine sediments from modern restricted basins
536 such as the Black Sea (Neubert et al. 2008) are ideal candidates for capturing the contemporaneous
537 seawater $\delta^{98}\text{Mo}$ (as well as Kyllaren fjord [Noordmann et al. 2015] and Lake Rogoznica [Bura-Nakić et
538 al. 2018]). This is so because minimized recharge of Mo from the open ocean into these settings
539 strengthens the possibility of near-quantitative Mo transfer from marine bottom waters to sediments.
540 Therefore, although these sedimentary enrichments may undersell the true size of the coeval global
541 seawater Mo reservoir, shales deposited at these times may be ideal candidates for capturing the coeval
542 global seawater $\delta^{98}\text{Mo}$.

543 If shales deposited between the purported OOE's from the Wuhe site did faithfully capture the
544 coeval seawater $\delta^{98}\text{Mo}$, then that composition was generally very light ($\delta^{98}\text{Mo}_{\text{SW}} \leq 0.94 \pm 0.10\text{‰}$; 2SD).
545 We indicate “generally” because our low-resolution study of shales at the Wuhe site (one sample about
546 every two meters) is very likely to leave large expanses of Ediacaran time unaccounted for – millions of
547 years in some cases, based on sample age estimates from Sahoo et al. (2016). Furthermore, two shale
548 samples from the Wuhe site that may have been deposited outside of the OOE's have heavier $\delta^{98}\text{Mo}$ (1.47
549 $\pm 0.10\text{‰}$; 2SD at 13.7m and $2.24 \pm 0.10\text{‰}$; 2SD at 110.7m) and may signify short-lived increases to the

550 coeval seawater $\delta^{98}\text{Mo}$. Alternatively, these heavier $\delta^{98}\text{Mo}$ may actually be from shale samples deposited
551 near the termination or shortly after the onset of the OOE. This scenario is possible because the two
552 shale samples from Wuhe with comparatively heavy $\delta^{98}\text{Mo}$ are located immediately before or after the
553 purported OOE (according the OOE locations proposed in Sahoo et al. [2016]; Fig. 3). Nevertheless,
554 generally lighter seawater $\delta^{98}\text{Mo}$ estimates inferred from the vast majority of shales deposited outside of
555 the OOE may indicate generally lower global ocean O_2 contents at these times.

556

557 5. Conclusions

558 Our new Mo isotope data help us argue that local controls in the Ediacaran Nanhua Basin played
559 important roles in driving some of the geochemical trends in black shales of the Doushantuo Formation
560 from South China. In particular, the transient development of an Mn oxide shuttle and changes in the
561 extent of tetrathiomolybdate formation linked to sulfide availability are both supported by the extremely
562 negative shale $\delta^{98}\text{Mo}$ excursions reported here. Coeval RSE patterns and accompanying Fe speciation
563 data from the same sedimentary rocks, although not originally interpreted in this manner (Sahoo et al.
564 2012, 2016), are also consistent with this hypothesis.

565 Importantly, enhanced oceanic oxygenation during the Ediacaran is still required to explain some
566 of the geochemical patterns in the Doushantuo Formation (i.e., those found in Sahoo et al. 2012, 2016),
567 despite the local redox-related complications identified here. Elevated Re and U abundances are
568 particularly difficult to explain without invoking global-scale oceanic oxygenation because oxide
569 shuttling and changes in local sulfide availability are not adequate to enrich these two metals to the levels
570 found in the Doushantuo Formation.

571 In light of our new data, it is worth reconsidering whether the Nanhua Basin maintained an
572 uninterrupted connection with the open ocean during the entirety of the Ediacaran Period. If the Nanhua
573 Basin was well-connected to the open ocean throughout the Ediacaran (as is assumed in previous work
574 [Sahoo et al. 2012, 2016]), then:

575

- 576 (1) Redox-sensitive element abundances in organic-rich shales from the Doushantuo
577 Formation should scale with coeval levels of global ocean oxygenation. Elevated RSE
578 abundances would signify a better oxygenated global ocean, while muted RSE
579 abundances would be indicative of a relatively less oxygenated one (i.e., the original
580 hypothesis of Sahoo et al. [2016]);
- 581 (2) Negative $\delta^{98}\text{Mo}$ excursions are likely a consequence of chemocline deepening in the
582 basin (**Section 4.3.1.**; and also see the leftmost panels in Fig. 10). When the chemocline

583 deepened, more sediments on the slope of the basin would have been exposed to oxic or
584 suboxic conditions. Shuttling of Mo to sediments by Mn oxides would be more likely
585 under these conditions. Sedimentary sulfide contents may also have diminished under
586 these conditions, in turn promoting incomplete tetrathiomolybdate formation. Both of
587 these processes are known to stimulate retention of lighter-mass Mo isotopes in marine
588 sediments and may thus explain the negative $\delta^{98}\text{Mo}$.

589 (3) Positive $\delta^{98}\text{Mo}$ found in organic-rich euxinic shales deposited between the OOEes are
590 likely a consequence of chemocline shallowing. When the chemocline shallowed, more
591 sediments on the slope of the basin would have been exposed to euxinic conditions.
592 Shuttling of Mo to sediments by Mn oxides would have been less likely under these
593 conditions. An associated increase in local sulfide availability would have also favored
594 more complete tetrathiomolybdate formation. Neither of these processes would have
595 favored the retention of lighter-mass Mo isotopes in marine sediments. The positive
596 $\delta^{98}\text{Mo}$ in these shales are most likely closer to matching the coeval ancient seawater
597 composition. Unfortunately, it is difficult to tell if the true seawater $\delta^{98}\text{Mo}$ is recorded.
598 Modern marine basins that maintain a strong connection with the open ocean never
599 capture the coeval seawater $\delta^{98}\text{Mo}$ and instead capture a large range of isotopically
600 lighter values (summarized by Kendall et al. 2017). By analogy, the organic-rich shales
601 of the Doushantuo may also capture fractionated Mo isotope values.

602
603 Alternatively, if the connection between this basin and the open-ocean was not always strong during the
604 Ediacaran (**Section 4.3.2.**; and also see the center panels in Fig. 10), then:

605
606 (1) Organic-rich shales of the Doushantuo Formation deposited during sea level highstands
607 would be the best candidates to preserve the remnants of open-ocean chemistry, as
608 viewed from the perspective of RSE enrichments. This likelihood is because the Nanhua
609 Basin would have been most strongly connected to the open ocean at these times. By
610 contrast, muted RSE enrichments in shales deposited during sea level lowstands would
611 not be as likely to preserve information about the RSE reservoir of the open-ocean. This
612 possibility is especially true if the Nanhua Basin was at times strongly restricted and
613 exchanged little or no seawater with the open ocean.

614 (2) Negative $\delta^{98}\text{Mo}$ excursions are likely a consequence of open-ocean seawater inflow
615 events into an otherwise restricted basin – similar to what happens today in the Baltic Sea
616 (Scholz et al. 2018). During transgressions, inflow of oxic open-ocean surface waters to

617 the basin could have stimulated the operation of a local Mn oxide shuttle, while also
618 exposing more sediments on the slope to oxic or suboxic conditions. Again, lighter-mass
619 Mo isotopes would be preferentially retained in sediments due to these processes.
620 (3) Positive $\delta^{98}\text{Mo}$ found in organic-rich shales during marine regressions are, again,
621 primarily a result of the termination of the processes driving the extremely negative
622 $\delta^{98}\text{Mo}$ excursions. However, if these shales were deposited in a strongly restricted basin,
623 then they are strong candidates to preserve the coeval seawater $\delta^{98}\text{Mo}$ because restricted
624 euxinic basins are shown to sometimes capture the coeval seawater $\delta^{98}\text{Mo}$ today (Neubert
625 et al. 2008, Noordmann et al. 2015, Bura-Nakić et al. 2018). The majority of seawater
626 $\delta^{98}\text{Mo}$ inferred from these shales ($\delta^{98}\text{Mo}_{\text{SW}} \leq 0.94 \pm 0.10\text{‰}$; 2SD) are much lighter than
627 that of the modern ocean ($\delta^{98}\text{Mo}_{\text{SW}} = 2.34 \pm 0.10\text{‰}$ [Nägler et al. 2014]). Accordingly,
628 these lighter $\delta^{98}\text{Mo}$ may fingerprint a comparatively less oxygenated global ocean at that
629 time compared to the modern ocean.

630 Some combination of both scenarios could also explain the data.

631 Moving forward, it will be important to unmix or at least account for these local and global
632 complications and their links to geochemical trends in Ediacaran-aged sedimentary rocks. Constraining
633 the degree of restriction between the Ediacaran Nanhua Basin and the open ocean during the time
634 intervals between the purported OOE is of particular importance. To date, inferences about the state of
635 global marine redox conditions during the Ediacaran are based mostly on geochemical trends found in
636 shales of the Doushantuo Formation and their relationship to coeval open-ocean chemistry. Well-
637 documented contemporaneous shales from the multiple sections of Northwestern Canada (e.g., Johnston
638 et al. 2013, Miller et al. 2017) are another potentially attractive target for future paleoredox studies.
639 However, the Ediacaran-aged shales from Northwestern Canada offer their own challenges because they
640 are thought to have been deposited under primarily ferruginous conditions (based on Fe speciation data
641 [Johnston et al. 2013, Miller et al. 2017]), which limits the utility of paleoredox proxies such as Mo.

642

643 **References**

644 Algeo T. J. and Lyons, T. W. (2006) Mo-total organic carbon covariation in modern anoxic marine
645 environments: Implications for analysis of paleoredox and paleohydrographic conditions.
646 *Paleoceanography* **21**, PA1016.

- 647 Algeo T. J. and Tribovillard N. (2009) Environmental analysis of paleoceanographic systems based on
648 molybdenum-uranium covariation. *Chemical Geology* **268**, 211-225.
- 649 An Z., Jiang G., Tong J., Tian L., Ye Q., Song H. and Song H. (2015) Stratigraphic position of the
650 Ediacaran Miaohu biota and its constraints on the age of the upper Doushantuo $\delta^{13}\text{C}$ anomaly in
651 the Yangtze Gorges area, South China. *Precambrian Research* **271**, 243–253.
- 652 Arnold G. L., Anbar A. D., Barling J. and Lyons T. W. (2004) Molybdenum isotope evidence for
653 widespread anoxia in Mid-Proterozoic oceans. *Science* **304**, 87-90.
- 654 Azrieli-Tal I., Matthews A., Bar-Matthews M., Almogi-Labin A., Vance D., Archer C. and Teutsch N.
655 (2014) Evidence from molybdenum and iron isotopes and molybdenum-uranium covariation for
656 sulphidic bottom waters during Eastern Mediterranean sapropel S1 formation. *Earth and
657 Planetary Science Letters* **393**, 231-242.
- 658 Barling J., Arnold, G. L. and Anbar A. D. (2001) Natural mass-dependent variations in the isotopic
659 composition of molybdenum. *Earth and Planetary Science Letters* **193**, 447-457.
- 660 Bristow T. F., Kennedy M. J., Derkowski A., Droser M. L., Jiang G. and Creaser R. A. (2009)
661 Mineralogical constraints on the paleoenvironments of the Ediacaran Doushantuo Formation.
662 *Proceedings of the National Academy of Sciences* **106**, 13190-13195.
- 663 Bura-Nakić E., Andersen M. B., Archer C., de Souza G. F., Marguš M. and Vance D. (2018) Coupled
664 Mo-U abundances and isotopes in a small marine euxinic basin: Constraints on processes in
665 euxinic basins. *Geochimica et Cosmochimica Acta* **222**, 212-229.
- 666 Burdige D. J. (1993) The biogeochemistry of manganese and iron reduction in marine sediments. *Earth
667 Science Reviews* **35**, 249-284.
- 668 Calvert S. E. and Pedersen T. F. (1996) Sedimentary geochemistry of manganese: Implications for the
669 environment of formation of manganiferous black shales. *Economic Geology* **91**, 36-47.
- 670 Chen J. H., Edwards R. L. and Wasserburg G. J. (1986) ^{238}U , ^{234}U and ^{232}Th in seawater. *Earth and
671 Planetary Science Letters* **80**, 241-251.
- 672 Clarkson M. O., Stirling C. H., Jenkyns H. C., Dickson A. J., Porcelli D., Moy C. M., Pogge von
673 Strandmann P. A. E., Cooke I. R. and Lenton T. M. (2018) Uranium isotope evidence for two
674 episodes of deoxygenation during Oceanic Anoxic Event 2. *Proceedings of the National Academy
675 of Sciences* **115**, 2918–2923.

676 Collier R. W. (1984) Particulate and dissolved vanadium in the North Pacific Ocean. *Nature* **309**, 441-
677 444.

678 Condon D., Zhu M., Bowring S., Wang W., Yang A. and Jin Y. (2005) U-Pb ages from the
679 Neoproterozoic Doushantuo Formation, China. *Science* **308**, 95–98.

680 Crusius J., Calvert S., Pedersen T. and Sage D. (1996) Rhenium and molybdenum enrichments in
681 sediments as indicators of oxic, suboxic and sulfidic conditions of deposition. *Earth and*
682 *Planetary Science Letters* **145**, 65-78.

683 Dickson A. J., Jenkyns H. C., Porcelli D., van den Boorn S. and Idiz E. (2016) Basin-scale controls on the
684 molybdenum-isotope composition of seawater during Oceanic Anoxic Event 2 (Late Cretaceous).
685 *Geochimica et Cosmochimica Acta* **178**, 291-306.

686 Dickson A. J. (2017) A molybdenum-isotope perspective on Phanerozoic deoxygenation events. *Nature*
687 *Geoscience* **10**, 721-726.

688 Duan Y., Anbar A. D., Arnold G. L., Lyons T. W., Gordon G. W. and Kendall B. (2010) Molybdenum
689 isotope evidence for mild environmental oxygenation before the Great Oxidation Event.
690 *Geochimica et Cosmochimica Acta* **74**, 6655-6668.

691 Eckert, S., Brumsack, H.J., Severmann, S., Schnetger, B., März, C. and Fröllje, H. (2013) Establishment
692 of euxinic conditions in the Holocene Black Sea. *Geology* **41**, 431-434.

693 Erickson B. E. and Helz G. R. (2000) Molybdenum(VI) speciation in sulfidic waters: Stability and lability
694 of thiomolybdates. *Geochimica et Cosmochimica Acta* **64**, 1149-1158.

695 Fike D. A., Grotzinger J. P., Pratt L. M. and Summons R. E. (2006) Oxidation of the Ediacaran ocean.
696 *Nature* **444**, 744-747.

697 Gill B. C., Lyons T. W., Young S. A., Kump L. R., Knoll A. H. and Saltzman M. R. (2011) Geochemical
698 evidence for widespread euxinic in the Later Cambrian ocean. *Nature* **469**, 80-83.

699 Goldberg T., Archer C., Vance D. and Poulton S. W. (2009) Mo isotope fractionation during adsorption
700 to Fe (oxyhydr) oxides. *Geochimica et Cosmochimica Acta* **73**, 6502–6516.

701 Goldberg T., Archer C., Vance D., Thamdrup B., McAnena A. and Poulton S. W. (2012) Controls on Mo
702 isotope fractionations in a Mn-rich anoxic marine sediment, Gullmar Fjord, Sweden. *Chemical*
703 *Geology* **296-297**, 73-82.

- 704 Goldberg T., Gordon G., Izon G., Archer C., Pearce C. R., McManus J., Anbar A. D. and Rehkämper M.
705 (2013) Resolution of inter-laboratory discrepancies in Mo isotope data: an intercalibration.
706 *Journal of Analytical Atomic Spectrometry* **28**, 724-735.
- 707 Gomez M. L. and Hurtgen M. T. (2015) Sulfur isotope fractionation in modern euxinic systems:
708 implications for paleoenvironmental reconstructions of paired sulfate-sulfide isotope records.
709 *Geochimica et Cosmochimica Acta* **157**, 39-55.
- 710 Greaney A. T., Rudnick R. L., Gaschnig R. M., Whalen J. B., Luais B. and Clemens J. D. (2018)
711 Geochemistry of Molybdenum in the continental crust. *Geochimica et Cosmochimica Acta* **238**,
712 36-54.
- 713 Gregory D. D., Lyons T. W., Large R. R., Jiang G., Stepanov A. S., Diamond C. W., Figueroa M. C. and
714 Olin P. (2017) Whole rock and discrete pyrite geochemistry as complementary tracers of ancient
715 ocean chemistry: An example from the Neoproterozoic Doushantuo Formation, China.
716 *Geochimica et Cosmochimica Acta* **216**, 201-220.
- 717 Han T. and Fan H. (2015) Dynamic evolution of the Ediacaran ocean across the Doushantuo Formation,
718 South China. *Chemical Geology* **417**, 261-272.
- 719 Hardisty D. S., Riedinger N., Planavsky N. J., Asael D., Andren T., Jorgensen B. B. and Lyons T. W.
720 (2016) A Holocene history of dynamic water column redox conditions in the Landsort Deep,
721 Baltic Sea. *American Journal of Science* **316**, 713-745.
- 722 Hardisty D. S., Lyons T. W., Riedinger N., Isson T. T., Owens J. D., Aller R. C., Rye D. M., Planavsky
723 N. J., Reinhard C. T., Gill B. C., Masterson A. L., Asael D. and Johnston D. T. (2018) An
724 evaluation of sedimentary molybdenum and iron as proxies for pore fluid paleoredox conditions.
725 *American Journal of Science* **318**, 527-556.
- 726 Häusler K., Dellwig O., Schnetger B., Feldens P., Leipe T., Moros M., Pollehne F., Schönke M.,
727 Wegwerth A. and Arz H. W. (2018) Massive Mn carbonate formation in the Landsort Deep
728 (Baltic Sea): Hydrographic conditions, temporal succession, and Mn budget calculations. *Marine*
729 *Geology* **395**, 260-270.
- 730 Hein J. and Koschinsky A. (2014) Deep-ocean ferromanganese nodules and crusts, In: Scott, S. (Ed.),
731 Treatise on Geochemistry 2nd Edition (TGC2), New Volume on Geochemistry of Mineral
732 Deposits, 2nd edition. 273–291.

- 733 Heiser U., Neumann T., Scholten J. and Stüben D. (2001) Recycling of manganese from anoxic sediments
734 in stagnant basins by seawater inflow: a study of surface sediments from the Gotland Basin,
735 Baltic Sea. *Marine Geology* **177**, 151–166.
- 736 Helz G. R., Miller C. V., Charnock J. M., Mosselmans J. F. W., Patrick R. A. D., Garner C. D. and
737 Vaughan D. J. (1996) Mechanism of molybdenum removal from the sea and its concentration in
738 black shales: EXAFS evidence. *Geochimica et Cosmochimica Acta* **60**, 3631-3642.
- 739 Hetzel A., Böttcher M. E., Wortmann U. G. and Brumsack H. (2009) Paleo-redox conditions during OAE
740 2 reflected in Demerara Rise sediment geochemistry (ODP Leg 207). *Palaeogeography,*
741 *Palaeoclimatology, Palaeoecology* **273**, 302-328.
- 742 Huang J., Chu X., Lyons T. W., Planavsky N. J. and Wen H. (2013) A new look at saponite formation
743 and its implications for early animal records in the Ediacaran of South China. *Geobiology* **11**, 3–
744 14.
- 745 Huckriede H. and Meischner D. (1996) Origin and environment of manganese-rich sediments within
746 black-shale basin. *Geochimica et Cosmochimica Acta* **60**, 1399-1413.
- 747 Jiang G., Kaufman A. J., Christie-Blick N., Zhang S., Wu H. (2007) Carbon isotope variability across the
748 Ediacaran Yangtze platform in South China: Implications for a large surface-to-deep ocean $\delta^{13}\text{C}$
749 gradient. *Earth and Planetary Science Letters* **261**, 303-320.
- 750 Jiang G., Shi X., Zhang S., Wang Y. and Xiao S. (2011) Stratigraphy and paleogeography of the
751 Ediacaran Doushantuo Formation (ca. 635-551 Ma) in South China. *Gondwana Research* **19**,
752 831-849.
- 753 Jin C., Li C., Algeo T. J., O’Connell B., Cheng M., Shi W., Shen J. and Planavsky, N.J. (2018) Highly
754 heterogeneous “poikiloredox” conditions in the early Ediacaran Yangtze Sea. *Precambrian*
755 *Research* **311**, 157-166.
- 756 Johnston D. T., Poulton S. W., Tosca N. J., O’Brien T., Halverson G. P., Schrag D. P. and Macdonald F.
757 A. (2013) Searching for an oxygenation event in the fossiliferous Ediacaran of northwestern
758 Canada. *Chemical Geology* **362**, 273-286.
- 759 Kendall B., Komiya T., Lyons T. W., Bates S. M., Gordon G. W., Romaniello S. J., Jiang G., Creaser R.
760 A., Xiao S., McFadden K., Sawaki Y., Tahata M., Shu D., Han J., Li Y., Chu X. and Anbar, A.D.
761 (2015) Uranium and molybdenum isotope evidence for an episode of widespread ocean
762 oxygenation during the late Ediacaran Period. *Geochimica et Cosmochimica Acta* **156**, 173–193.

- 763 Kendall B., Dahl T. W. and Anbar A. D. (2017) Good golly, why Moly? The stable isotope geochemistry
764 of molybdenum. *Reviews in Mineralogy and Geochemistry* **82**, 682-732.
- 765 King E. K., Perakis S. S. and Pett-Ridge J. C. (2018) Molybdenum isotope fractionation during
766 adsorption to organic matter. *Geochimica et Cosmochimica Acta* **222**, 584-598.
- 767 King E. K. and Pett-Ridge J. C. (2018) Reassessing the dissolved molybdenum isotopic composition of
768 ocean inputs: The effect of chemical weathering and groundwater. *Geology* **46**, 955-958.
- 769 Knoll A. H. (2011) The multiple origins of complex multicellularity. *Annual Review of Earth and*
770 *Planetary Sciences* **39**, 217-239.
- 771 Lenton T. M., Boyle R. A., Poulton S. W., Shields-Zhou G. A. and Butterfield N. J. (2014) Co-evolution
772 of eukaryotes and ocean oxygenation in the Neoproterozoic era. *Nature Geoscience* **7**, 257.
- 773 Lenz C., Jilbert T., Conley D. J., Wolthers M. and Slomp C. P. (2015) Are recent changes in sediment
774 manganese sequestration in the euxinic basins of the Baltic Sea linked to the expansion of
775 hypoxia? *Biogeosciences* **12**, 4875-4894.
- 776 Lowenstein T. K., Kendall B. and Anbar A. D. (2013) The geologic history of seawater. In *Treatise on*
777 *Geochemistry: Second Edition* 8, 569-622. Elsevier Inc. doi: 10.1016/B978-0-08-095975-
778 7.00621-5.
- 779 McFadden K. A., Huang J., Chu X., Jiang G., Kaufman A. J., Zhou C., Yuan X. and Xiao S. (2008)
780 Pulsed oxidation and biological evolution in the Ediacaran Doushantuo Formation. *Proceedings*
781 *of the National Academy of Sciences* **105**, 3197-3202.
- 782 Meyer K. M. and Kump L. R. (2008) Oceanic euxinia in Earth history: Causes and consequences. *Annual*
783 *Review of Earth and Planetary Science* **36**, 251-288.
- 784 Miller A. J., Strauss J. V., Halverson G. P., Macdonald F. A., Johnston D. T. and Sperling E. A. (2017)
785 Tracking the onset of Phanerozoic-style redox-sensitive trace metal enrichments: New results
786 from basal Ediacaran post-glacial strata in NW Canada. *Chemical Geology* **457**, 24-37.
- 787 Miller C. A., Peucker-Ehrenbrink B., Walker B. D. and Marcantonio F. (2011) Re-assessing the surface
788 cycling of molybdenum and rhenium. *Geochimica et Cosmochimica Acta* **75**, 7146-7179.
- 789 Morford J. L. and Emerson E. (1999) The geochemistry of redox sensitive trace metals in sediments.
790 *Geochimica et Cosmochimica Acta* **63**, 1735-1750.

- 791 Morford J. L., Emerson S. R., Breckel E. J. and Kim S. H. (2005) Diagenesis of oxyanions (V, U, Re,
792 ,and Mo) in pore waters and sediments from a continental margin. *Geochimica et Cosmochimica*
793 *Acta* **69**, 5021-5032.
- 794 Morris A. W. (1975) Dissolved molybdenum and vanadium in the northeast Atlantic Ocean. *Deep-Sea*
795 *Research* **22**, 49-54.
- 796 Nägler T. F., Neubert N., Bottcher M. E., Dellwig O. and Schnetger B. (2011) Molybdenum isotope
797 fractionation in pelagic euxinia: evidence from the modern Black and Baltic Seas. *Chemical*
798 *Geology* **289**, 1-11.
- 799 Nägler T. F., Anbar A. D., Archer C., Goldberg T., Gordon G. W., Greber N. D., Siebert C., Sohrin Y.
800 and Vance D. (2014) Proposal for an international molybdenum isotope measurement standard
801 and data representation. *Geostandards and Geoanalytical Research* **38**, 149–151.
- 802 Nameroff T. J., Balistrieri L. S. and Murray J. W. (2002) Suboxic trace metal geochemistry in the eastern
803 tropical North Pacific. *Geochimica et Cosmochimica Acta* **66**, 1139-1158.
- 804 Neubert N., Nägler T. F. and Böttcher M. E. (2008) Sulfidity controls molybdenum isotope fractionation
805 into euxinic sediments: Evidence from the modern Black Sea. *Geology* **36**, 775-778.
- 806 Noordmann J., Weyer S., Montoya-Pino C., Dellwig O., Neubert N., Eckert S., Paetzel M. and Böttcher
807 M. E. (2015) Uranium and molybdenum isotope systematics in modern euxinic basins: case
808 studies from the central Baltic Sea and the Kyllaren fjord (Norway). *Chemical Geology* **396**, 182-
809 195.
- 810 Och L. M., Cremonese L., Shields-Zhou G. A., Poulton S. W., Struck U., Ling H., Li D., Chen X.,
811 Manning C. A., Thirlwall M., Strauss H. and Zhu M. (2016) Paleooceanographic controls on
812 spatial redox distribution over the Yangtze Platform during the Ediacaran-Cambrian transition.
813 *Sedimentology* **63**, 378-410.
- 814 Olson S. L., Ostrander C. M., Gregory D. D., Roy M., Anbar A. D. and Lyons T. W. (2019) Volcanically
815 modulated pyrite burial and ocean-atmosphere oxidation. *Earth and Planetary Science Letters*
816 **506**, 417-427.
- 817 Owens J. D., Lyons T. W., Li X., Macleod K. G., Gordon G., Kuypers M. M. M., Anbar A., Kuhnt W.
818 and Severmann S. (2012) Iron isotope and trace metal records of iron cycling in the proto-North
819 Atlantic during the Cenomanian-Turonian oceanic anoxic event (OAE-2). *Paleoceanography* **27**,
820 doi: 10.1029/2012PA002328.

821 Owens J. D., Gill B. C., Jenkyns H. C., Bates S. M., Severmann S., Kuypers M. M. M., Woodfine R. G.
822 and Lyons T. W. (2013) Sulfur isotopes track the global extent and dynamics of euxinia during
823 Cretaceous Oceanic Anoxic Event 2. *Proceedings of the National Academy of Sciences* **110**,
824 18407-18412.

825 Owens J. D., Reinhard C. T., Rohrssen M., Love G. D. and Lyons T. W. (2016) Empirical links between
826 trace metal cycling and marine microbial ecology during a large perturbation to Earth's carbon
827 cycle. *Earth and Planetary Science Letters* **449**, 407-417.

828 Owens J. D., Lyons T. W. and Lowery C. M. (2018) Quantifying the missing sink for global organic
829 carbon burial during a Cretaceous oceanic anoxic event. *Earth and Planetary Science Letters* **499**,
830 83-94.

831 Partin C. A., Bekker A., Planavsky N. J., Scott C. T., Gill B. C., Li C., Podkovyrov V., Maslov A.,
832 Konhauser K. O., Lalonde S. V., Love G. D., Poulton S. W. and Lyons T. W. (2013) Large-scale
833 fluctuations in Precambrian atmospheric and oceanic oxygen levels from the record of U in
834 shales. *Earth and Planetary Science Letters* **369-370**, 284-293.

835 Poulson R. L., Siebert C., McManus J. and Berelson W. M. (2006) Authigenic molybdenum isotope
836 signatures in marine sediments. *Geology* **34**, 617-620.

837 Poulson Brucker R. L., McManus J., Severmann S. and Berelson W. M. (2009) Molybdenum behavior
838 during early diagenesis: insights from Mo isotopes. *Geochemistry Geophysics Geosystems* **10**,
839 Q06010.

840 Raiswell R., Hardisty D. S., Lyons T. W., Canfield D. E., Owens J. D., Planavsky N. J., Poulton S. W.
841 and Reinhard C. T. (2018) The iron paleoredox proxies: a guide to pitfalls, problems and proper
842 practice. *American Journal of Science* **318**, 491-526.

843 Reinhard C. T., Planavsky N. J., Robbins L. J., Partin C. A., Gill B. C., Lalonde S. V., Bekker A.,
844 Konhauser K. O. and Lyons T. W. (2013) Proterozoic ocean redox and biogeochemical stasis.
845 *Proceedings of the National Academy of Sciences* **111**, 5357-5362.

846 Reinhard C. T., Planavsky N. J., Olson S. L. and Lyons T. W. (2016) Earth's oxygen cycle and the
847 evolution of animal life. *Proceedings of the National Academy of Sciences* **113**, 8933-8938.

848 Rudnick R. L. and Gao S. (2003) Composition of the continental crust. In *The Crust*, vol. 3 (ed. R.L.
849 Rudnick). Elsevier, 1-64.

850 Sahoo S. K., Planavsky N. J., Kendall B., Wang X., Shi X., Scott C., Anbar A. D., Lyons T. W. and Jiang
851 G. (2012) Ocean oxygenation in the wake of the Marinoan glaciation. *Nature* **489**, 546–549.

852 Sahoo S. K. (2015) Ediacaran ocean redox evolution. UNLV Theses. Dissertations, Professional Papers,
853 and Capstones (Paper 2577).

854 Sahoo S. K., Planavsky N. J., Jiang G., Kendall B., Owens J. D., Wang X., Shi X., Anbar A. D. and
855 Lyons T. W. (2016) Oceanic oxygenation events in the anoxic Ediacaran ocean. *Geobiology* **14**,
856 457-468.

857 Schneider, A., Tanhua, T., Roether, W. and Steinfeldt, R. (2014) Changes in ventilation of the
858 Mediterranean Sea during the past 25 year. *Ocean Science* **10**, 1-16.

859 Scholz F., Hensen C., Noffke A., Rohde A., Liebetrau V. and Wallmann K. (2011) Early diagenesis of
860 redox-sensitive trace metals in the Peru upwelling area – response to ENSO-related oxygen
861 fluctuations in the water column. *Geochimica et Cosmochimica Acta* **75**, 7257-7276.

862 Scholz F., McManus J. and Sommer S. (2013) The manganese and iron shuttle in a modern euxinic basin
863 and implications for molybdenum cycling at euxinic ocean margins. *Chemical Geology* **355**, 56–
864 68.

865 Scholz F., Siebert C., Dale A. W. and Frank M. (2017) Intense molybdenum accumulation in sediments
866 underneath a nitrogenous water column and implications for the reconstruction of paleo-redox
867 conditions based on molybdenum isotopes. *Geochimica et Cosmochimica Acta* **213**, 400-417.

868 Scholz F., Baum M., Siebert C., Eroglu S., Dale A. W., Naumann M. and Sommer S. (2018) Sedimentary
869 molybdenum cycling in the aftermath of seawater inflow to the intermittently euxinic Gotland
870 Deep, Central Baltic Sea. *Chemical Geology* **491**, 27-38.

871 Scott C., Lyons T. W., Bekker A., Shen Y., Poulton S. W., Chu X. and Anbar, A.D. (2008) Tracing the
872 stepwise oxygenation of the Proterozoic ocean. *Nature* **452**, 456–459.

873 Scott C., Slack J. F. and Kelley K. D. (2017) The hyper-enrichment of V and Zn in black shales of the
874 Late Devonian-Early Mississippian Bakken Formation (USA). *Chemical Geology* **452**, 24-33.

875 Sheen A. I., Kendall B., Reinhard C. T., Creaser R. A., Lyons T. W., Bekker A., Poulton S. W. and Anbar
876 A. D. (2018) A model for the oceanic mass balance of rhenium and implications for the extent of
877 Proterozoic ocean anoxia. *Geochimica et Cosmochimica Acta* **227**, 75-95.

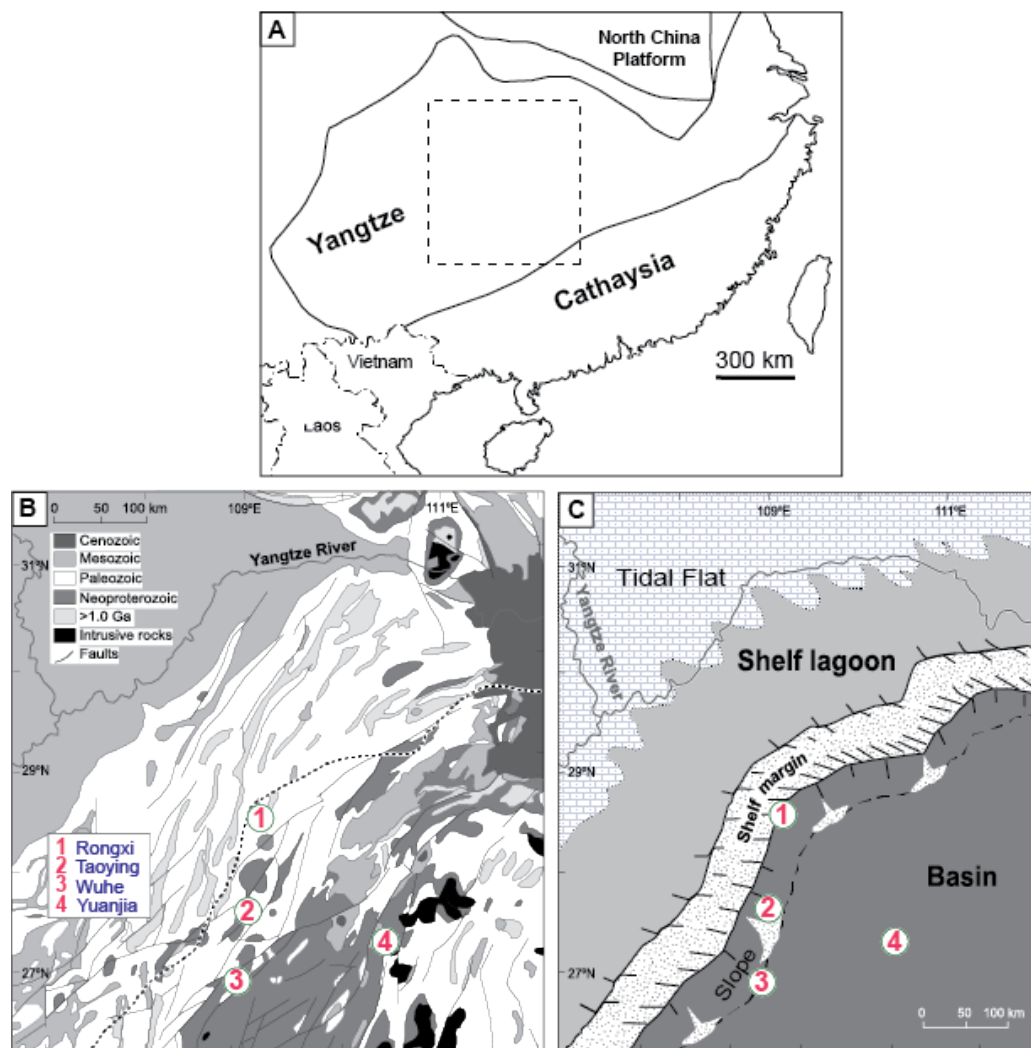
- 878 Siebert C., Nögler T. F., Kramers J. D. (2001) Determination of the molybdenum isotope fractionation by
879 double-spike multicollector inductively coupled plasma mass spectrometry. *Geochemistry,*
880 *Geophysics, and Geosystems* 2:2000GC000124.
- 881 Sperling E. A., Wolock C. J., Morgan A. S., Gill B. C., Kunzmann M., Halverson G. P., Macdonald F. A.,
882 Knoll A. H. and Johnston D. T. (2015) Statistical analysis of iron geochemical data suggests
883 limited late Proterozoic oxygenation. *Nature* **523**, 451-454.
- 884 Tossell J. A. (2005) Calculating the partitioning of the isotopes of Mo between oxidic and sulfidic species
885 in aqueous solution. *Geochimica et Cosmochimica Acta* **69**, 2981–2993.
- 886 Tribovillard N., Algeo T. J., Lyons T. W. and Riboulleau A. (2006) Trace metals as paleoredox and
887 paleoproductivity proxies: An update. *Chemical Geology* **232**, 12-32.
- 888 Volkov I. I. (2000) Dissolved inorganic carbon and its isotopic composition in the waters of anoxic
889 marine basin. *Oceanology* **40**, 499-502.
- 890 Wang L., Shi X. and Jiang G. (2012) Pyrite morphology and redox fluctuations recorded in the Ediacaran
891 Doushantuo Formation. *Palaeogeography, Palaeoclimatology, Palaeoecology* **333**, 218-227.
- 892 Wang X., Jiang G., Shi X. and Xiao S. (2016) Paired carbonate and organic carbon isotope variations of
893 the Ediacaran Doushantuo Formation from an upper slope section at Siduping, South China.
894 *Precambrian Research* **273**, 53-66.
- 895 Wasylenki L. E., Rolfe B. A., Weeks C. L., Spiro T. G. and Anbar A. D. (2008) Experimental
896 investigation of the effects of temperature and ionic strength on Mo isotope fractionation during
897 adsorption to manganese oxides. *Geochimica et Cosmochimica Acta* **72**, 5997-6005.
- 898 Willbold M. and Elliot T. (2017) Molybdenum isotope variations in magmatic rocks. *Chemical Geology*
899 **449**, 253-268.

900

901 **Acknowledgements**

902 We would like to thank Wang Zheng for his help with instrumental analysis at Arizona State
903 University. This research was supported financially by the NSF Frontiers in Earth System Dynamics
904 program award NSF EAR-1338810 (C.M.O., T.W.L., and A.D.A.), the Natural Sciences and Engineering
905 Research Council of Canada (NSERC) Discovery Grant RGPIN-435930 (B.K.), the Earth-Life
906 Transitions Program of the U.S. National Science Foundation (T.W.L. and N.J.P.) and the NASA

907 Astrobiology Institute under Cooperative Agreement No. NNA15BB03A issued through the Science
908 Mission Directorate (T.W.L, N.J.P., and A.D.A.). This material is based upon work supported by the
909 National Science Foundation Graduate Research Fellowship Program under Grant No. 026257-001
910 (C.M.O.). Any opinions, findings, and conclusions or recommendations expressed in this material are
911 those of the authors and do not necessarily reflect the views of the National Science Foundation.



912

913 **Figure 1. Tectonic, geological, and paleogeographic maps for the Yangtze platform of South China.**

914 (a) Tectonic map showing the Yangtze and Cathaysia blocks in China, with the dashed rectangle

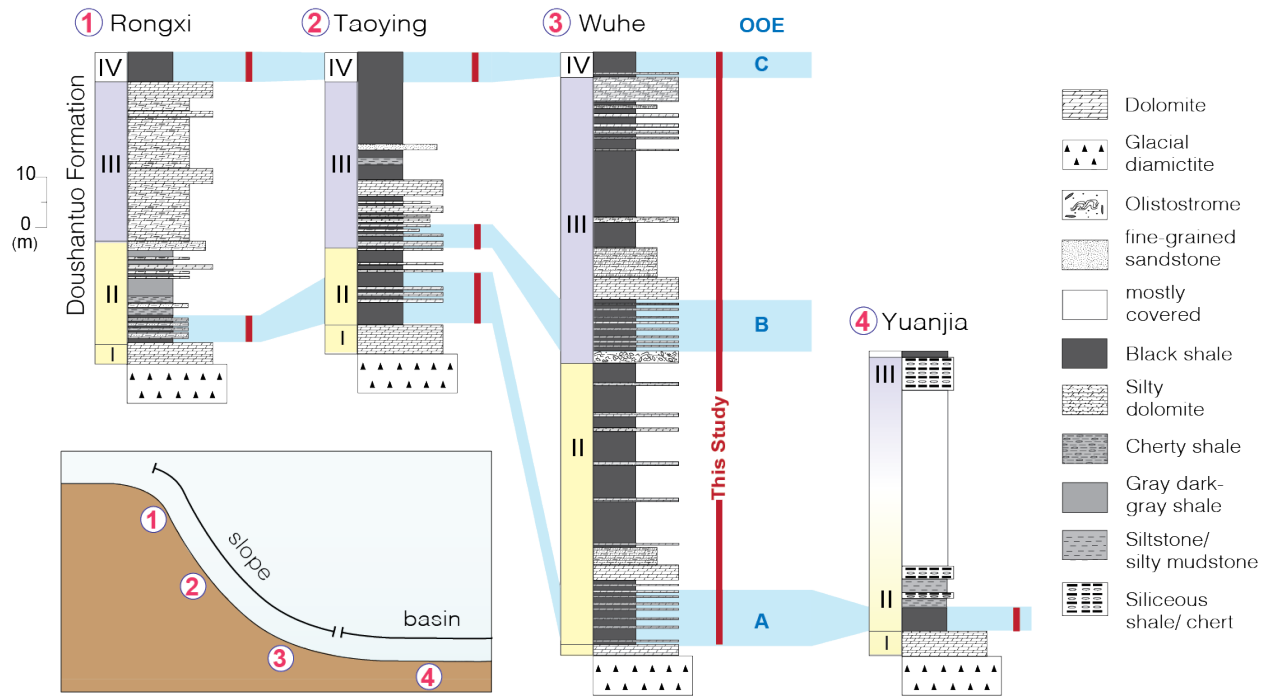
915 corresponding to the area depicted in B and C. (b) Simplified geological map showing exposures of strata

916 in the central Yangtze platform of South China. The dotted line signifies the position of the platform

917 margin during the late Neoproterozoic, and each number represents a site from which shales used in this

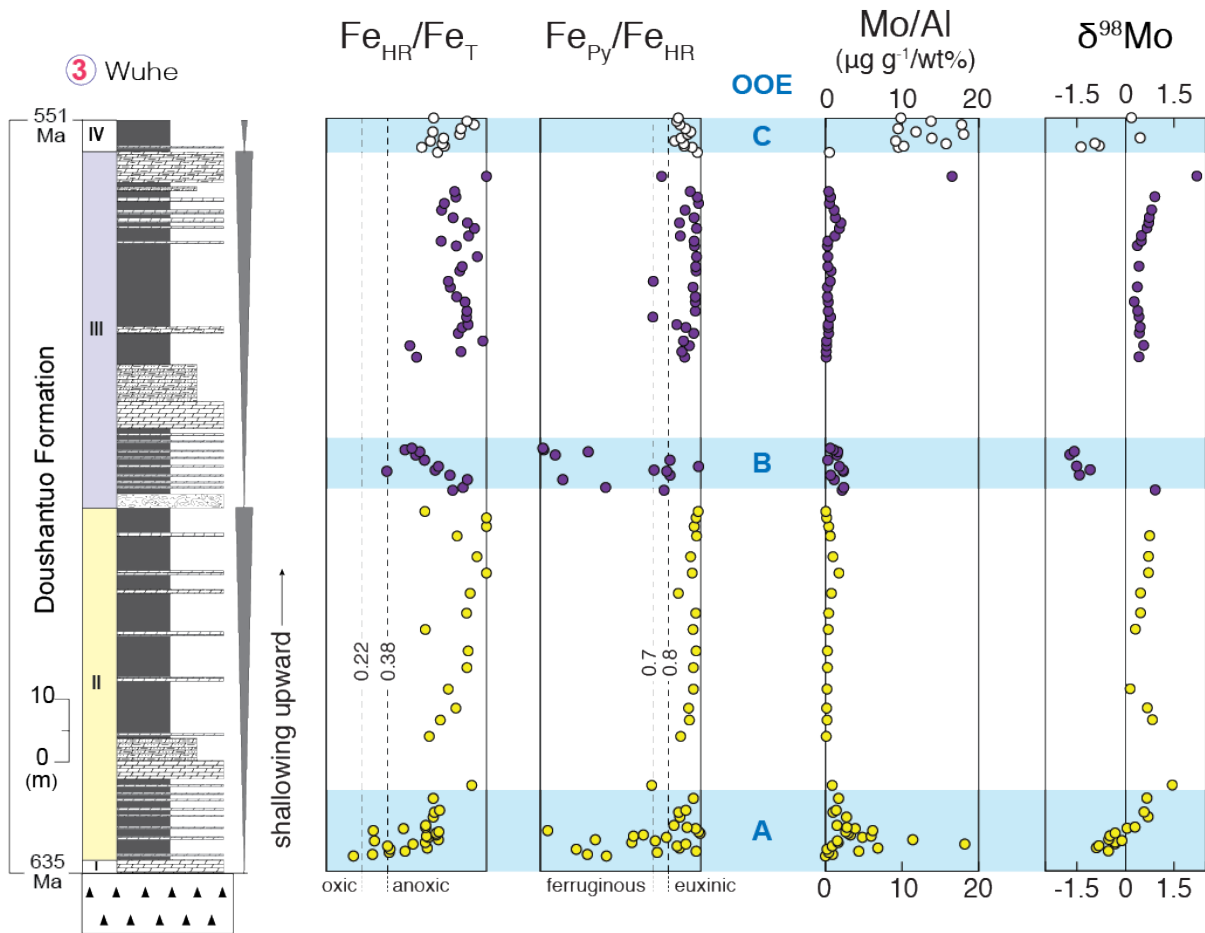
918 study were originally collected. (c) Paleogeographic reconstruction of the Nanhua Basin during the

919 Ediacaran Period. Figures modified from Jiang et al. (2011).



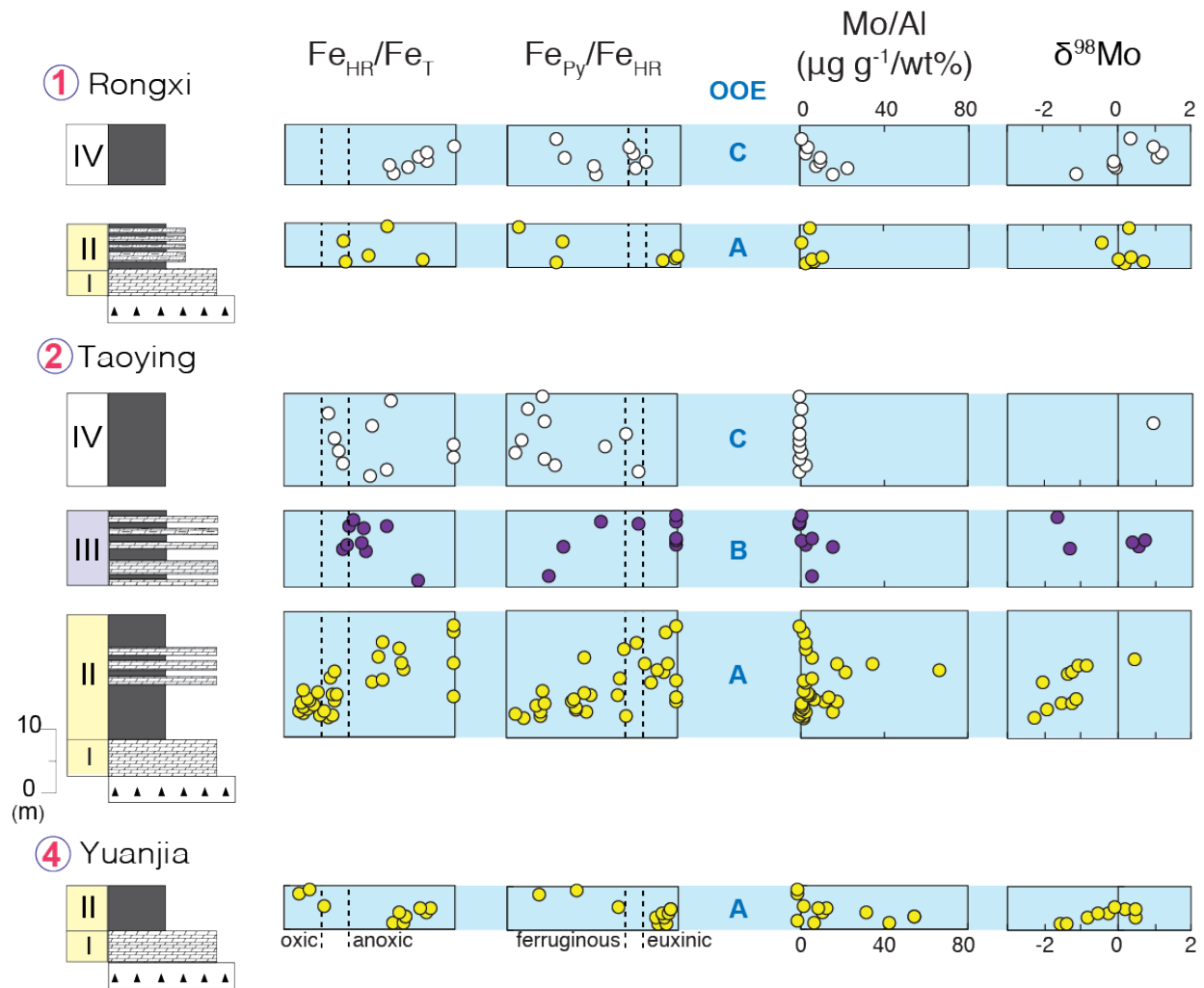
920

921 **Figure 2. Sections analyzed in this study.** For a detailed description of lithology, see Jiang et al. (2011)
 922 and Sahoo et al. (2012). Section intervals targeted here are signified by the vertical red bar. Previously
 923 identified Ediacaran ocean oxygenation events (OOEs) are identified by blue boxes (A, B, and C [Sahoo
 924 et al. 2011, 2016]). Stratigraphic columns, slope reconstruction, and legend are modified from Jiang et al.
 925 (2011) and Sahoo et al. (2016).



926

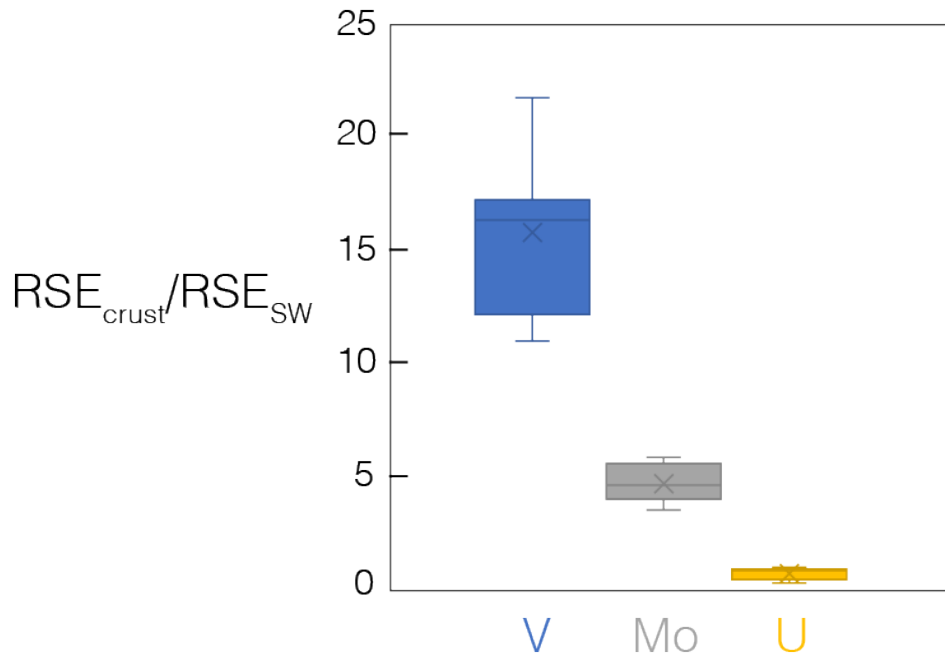
927 **Figure 3. Geochemistry of the Wuhe section.** Iron speciation and trace metal data is from Sahoo et al.
 928 (2012, 2016). Thresholds for anoxic and euxinic deposition are adapted from Raiswell et al. (2018).
 929 Again, blue boxes signify purported OOE. Data points are color-coded according to Doushantuo
 930 Member. See Fig. 1 for a lithology key. All error bars represent the 2SD reproducibility of that sample or
 931 the external long-term reproducibility of natural reference materials, whichever is greater. In most cases,
 932 error bars are smaller than the data points. Figure modified from Sahoo et al. (2016).



933

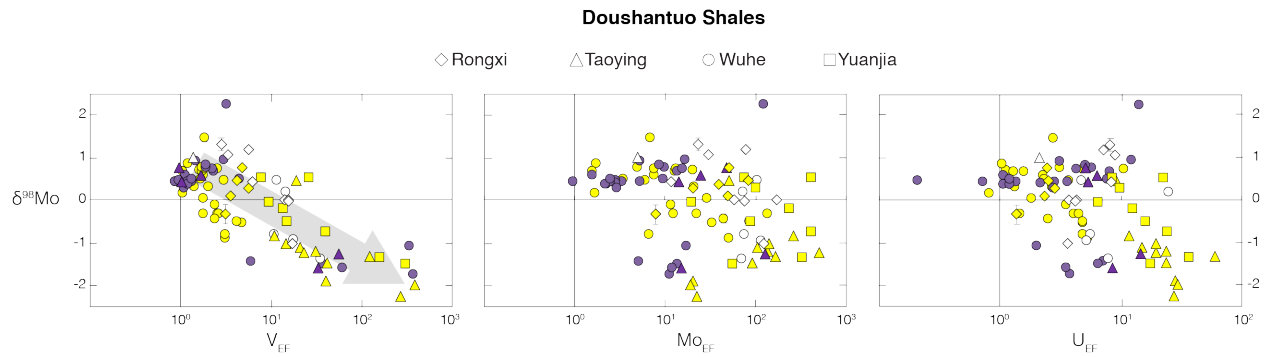
934 **Figure 4. Geochemistry of the Rongxi, Taoying, and Yuanjia sections.** Iron speciation and trace metal
 935 data is from Sahoo et al. (2012, 2016) and Sahoo (2015). Thresholds for anoxic and euxinic deposition are
 936 adapted from Raiswell et al. (2018). Again, blue boxes signify purported OOE and data points are color-
 937 coded according to Doushantuo Member. See Fig. 1 for a lithology key. All error bars represent the 2SD
 938 reproducibility of that sample or the external long-term reproducibility of natural reference materials,
 939 whichever is greater. In most cases, error bars are smaller than the data points. Figure modified from
 940 Sahoo et al. (2012).

Modern ferromanganese crusts



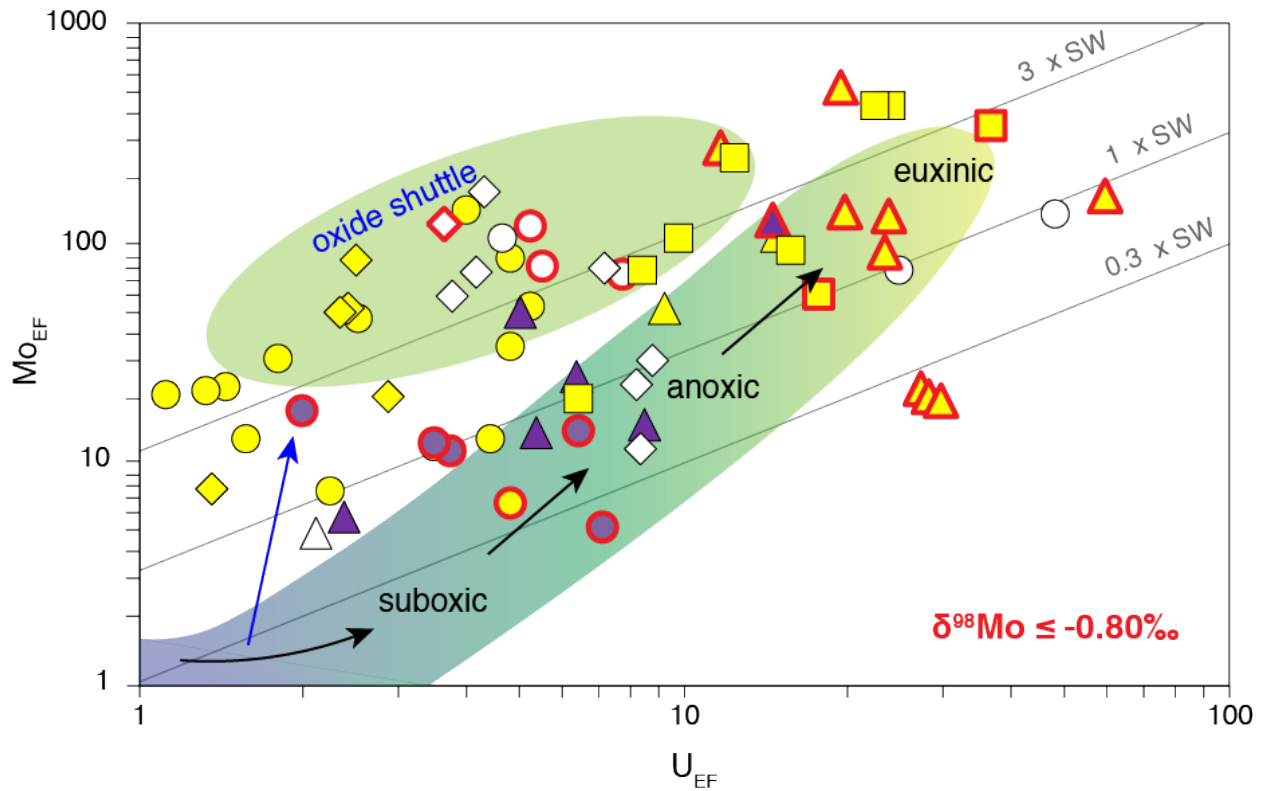
941

942 **Figure 5. Whisker plots showing relative abundance of redox-sensitive elements (RSEs) in modern**
943 **seawater and ferromanganese crusts.** Seawater RSE concentrations (in nmol/kg [Morris 1975, Collier
944 1984, and Chen et al. 1986]) and ferromanganese crust RSE abundances (in $\mu\text{g/g}$ [Hein and Koschinsky
945 2014]) come from previous work. Whisker plots represent the range of values when dividing the average
946 RSE abundances from ferromanganese crusts from different sites (Table 1, Hein and Koschinsky [2014])
947 by the average seawater concentration of that RSE.



948

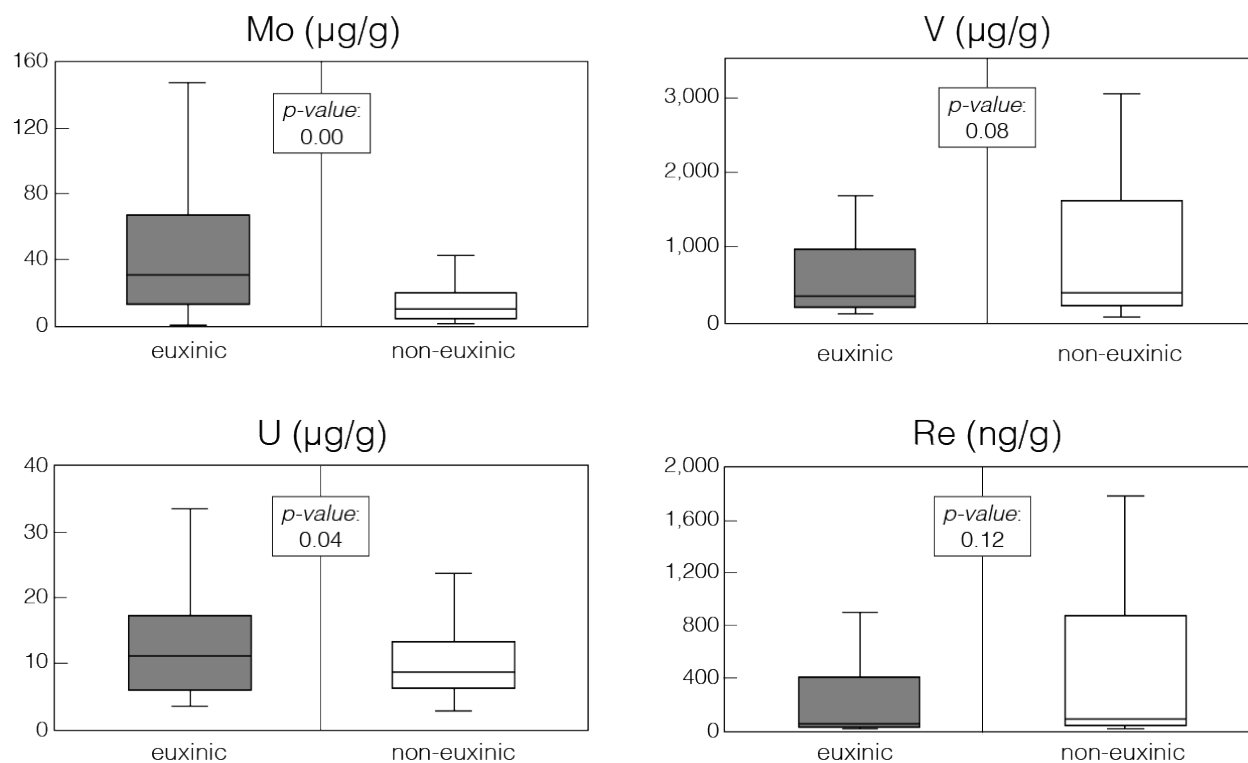
949 **Figure 6. Cross-plots of Mo isotope compositions and RSE enrichment factors (EF) in Doushantuo**
 950 **Shales.** Mo isotope data is from this study and elemental abundances come from previous work (Sahoo et
 951 al. 2012, 2016). Enrichment Factors were calculated relative to upper continental crust as follows: $RSE_{EF} = (RSE/Al)_{shale} \div (RSE/Al)_{upper\ crust}$ (RSE abundances in $\mu\text{g/g}$ and Al in wt%). Upper continental crust
 952 elemental abundances used in our calculations come from Rudnick and Gao (2003). Data point shapes
 953 coincide with the different sites from South China, and colors signify the different Doushantuo Members
 954 (II = yellow, III = purple, and IV = white).
 955



956

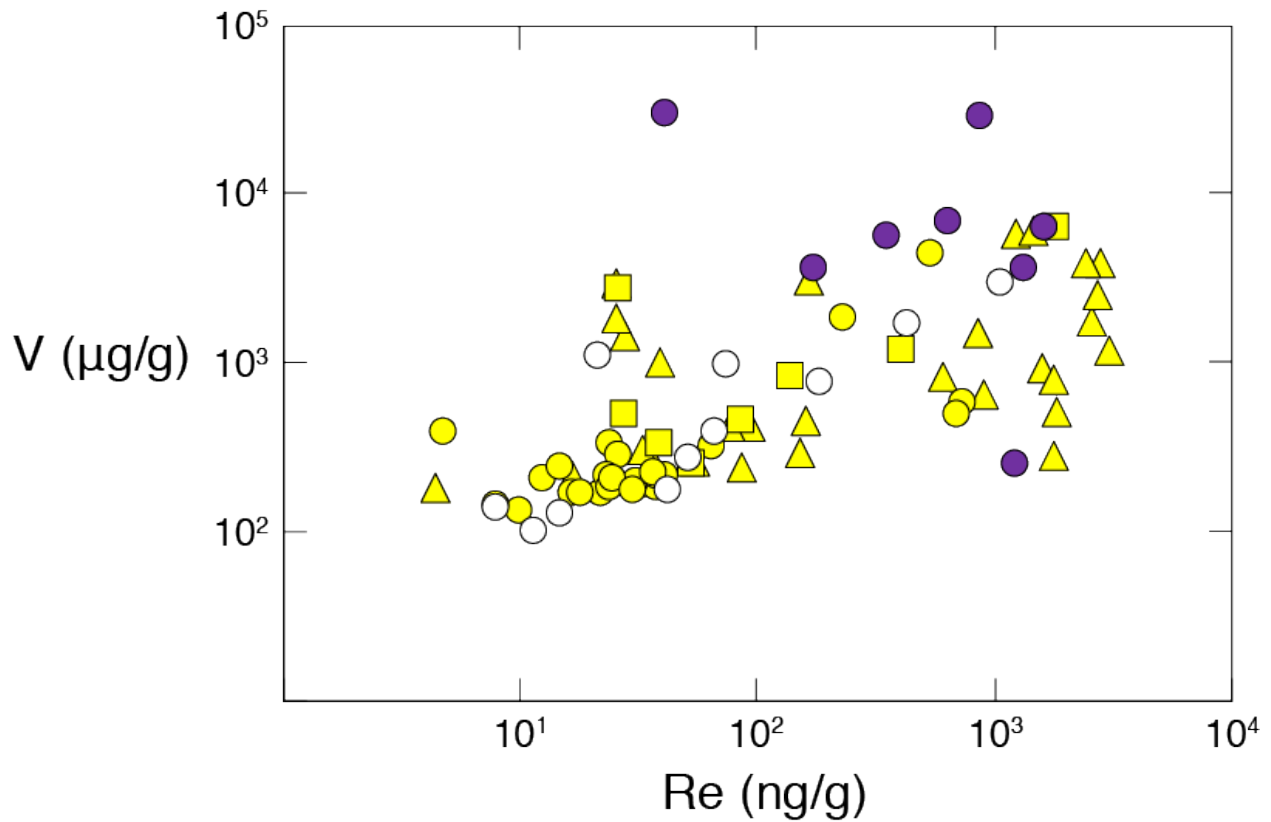
957 **Figure 7. Cross-plot of Mo and U enrichment Factors (EF) in Doushantuo Shales during OOE.**

958 Trace metal data in this plot comes from Sahoo et al. (2012, 2016) and Sahoo (2015). Enrichment Factors
 959 were calculated relative to upper continental crust as follows: $RSE_{EF} = (RSE/Al)_{shale} \div (RSE/Al)_{upper\ crust}$
 960 (RSE abundances in $\mu\text{g/g}$ and Al in wt%). Upper continental crust elemental abundances used in our
 961 calculations come from Rudnick and Gao (2003). Data point shapes coincide with the different sites from
 962 South China (diamonds = Rongxi, triangles = Taoying, circles = Wuhe, and squares = Yuanjia) and colors
 963 signify the different Doushantuo Members (II = yellow, III = purple, and IV = white). Shale samples with
 964 $\delta^{98}\text{Mo} \leq -0.80\text{‰}$ are outlined in red. Figure and fields are modified from Algeo and Tribovillard (2009)
 965 and Jin et al. (2018).



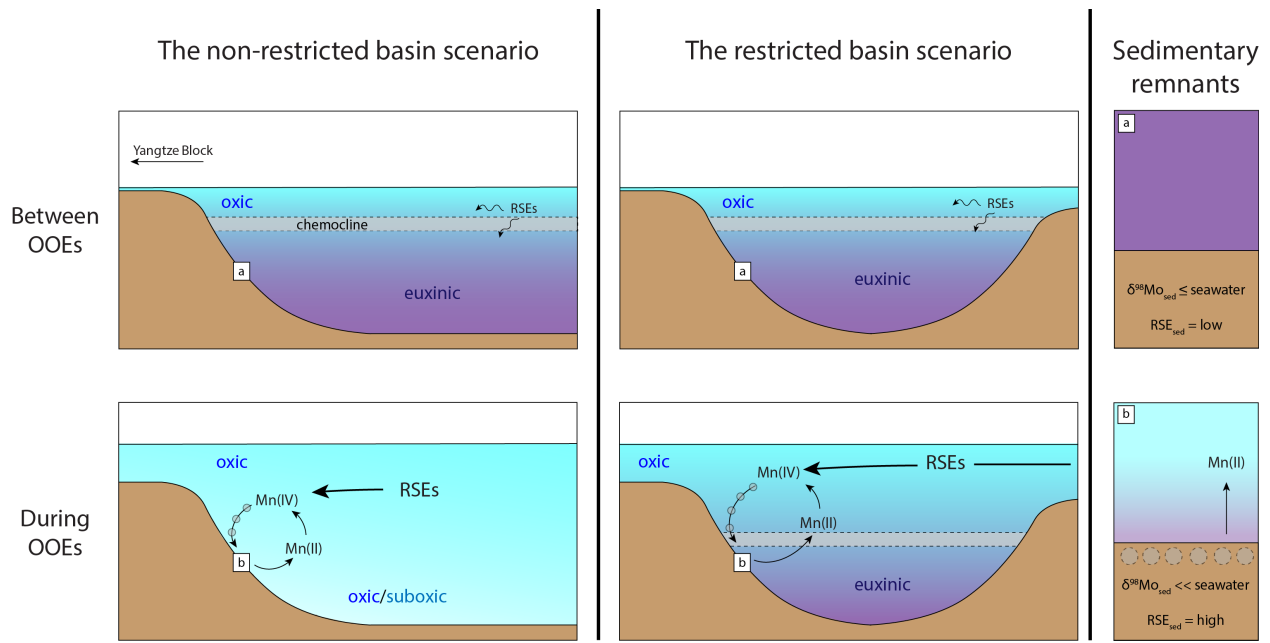
966

967 **Figure 8. Whisker plots showing RSE concentrations in Doushantuo shales during OOE according**
 968 **to local redox conditions.** Local redox conditions are determined by Fe speciation data (e.g., shale
 969 samples with $\text{Fe}_{\text{HR}}/\text{Fe}_{\text{T}} > 0.22$ and $\text{Fe}_{\text{Py}}/\text{Fe}_{\text{HR}} > 0.8$ are deemed euxinic in these plots). Data from all
 970 sections targeted in this study are included in the plots (i.e., Rongxi, Taoying, Wuhe, and Yuanjia). Iron
 971 speciation and RSE data is from Sahoo et al. (2012, 2016).



972

973 **Figure 9. Cross-plot of V and Re concentrations in Doushantuo Shales during OOE.** V and Re
 974 concentration data is from Sahoo et al. (2012, 2016). Data point shapes coincide with the different sites
 975 from South China (triangles = Taoying, circles = Wuhe, and squares = Yuanjia; similar to Fig. 6) and
 976 colors signify the different Doushantuo Members (II = yellow, III = purple, and IV = white).



977

978 **Figure 10. Possible evolution of seawater in the Ediacaran Nanhua Basin depending on the degree**
 979 **of connection between this basin and the open ocean.** The leftmost panels outline the possible
 980 evolution of seawater if the Nanhua Basin maintained an uninterrupted connection with the open ocean
 981 throughout the Ediacaran. The center panels outline this possible evolution if the Nanhua Basin was at
 982 times a restricted basin. Panels at the far right labeled “a” and “b” outline the associated sedimentary
 983 remnants on the slope of the paleo basin for each scenario (a = between OOE's and b = during OOE's).
 984 Grey circles represent insoluble Mn oxide minerals.